

Review on the structured light properties: rotational features and singularities

Oleg V. Angelsky^{a,b*}, Aleksandr Ya. Bekshaev^c, Igor I. Mokhun^b, Mikhail V. Vasnetsov^d,
Claudia Yu. Zenkova^{a,b}, Steen G. Hanson^e, Jun Zheng^a

^a Taizhou Research Institute of Zhejiang University, Taizhou, China,

^b Chernivtsi National University, Chernivtsi, Ukraine,

^c Physics Research Institute, Odessa I. I. Mechnikov National University, Odessa, Ukraine,

^d Department of Optical Quantum Electronics, Institute of Physics of the NAS of Ukraine, Kyiv, Ukraine

^e DTU Fotonik, Department of Photonics Engineering, DK-4000 Roskilde, Denmark

Article info

Article history:

Received 10 Dec. 2021

Received in revised form 4 Jan. 2022

Accepted 13 Jan. 2022

Available on-line 25 Mar. 2022

Keywords:

Singularity spin and orbital angular momentum; energy flow; structured light; optical vortices.

Abstract

The review exposes basic concepts and manifestations of the singular and structured light fields. The presentation is based on deep intrinsic relations between the singularities and the rotational phenomena in light; it involves essentially the dynamical aspects of light fields and their interactions with matter. Due to their topological nature, the singularities of each separate parameter (phase, polarization, energy flow, etc.) form coherent interrelated systems (singular networks), and the meaningful interconnections between the different singular networks are analysed. The main features of singular-light structures are introduced via generic examples of the optical vortex and circular vortex beams. The review describes approaches for generation and diagnostics of different singular networks and underlines the role of singularities in formation of optical field structures. The mechanical action of structured light fields on material objects is discussed on the base of the spin-orbital (canonical) decomposition of electromagnetic momentum, expressing the special roles of the spin (polarization) and spatial degrees of freedom. Experimental demonstrations spectacularly characterize the topological nature and the immanent rotational features of the light-field singularities. The review is based on the results obtained by its authors with a special attention to relevant works of other researchers.

1. Introduction

Commonly accepted concepts of light coming from everyday life evoke no associations with the rotational type of evolution. On the contrary, the light propagation provides bright examples of the rectilinear motion and is sometimes considered as the antipode to any circulation or vortex phenomena rather typical for “other”, non-optical physics. From this point of view, ideas on the “rotational” properties of light look rather strange, and for a long time these were far from the scientific mode of life. Probably, the first scientific ideas relating the rotational features of light go back to Descartes [1, 2]. In his metaphysical system, the rotational motion generally occupied an out-standing position; he conceived the light as compressions

of an absolutely elastic medium and explained the difference in colours by vortex motions of the medium particles performed with different velocities.

One may admire Descartes’ clairvoyance, but his anticipations were only speculations. The next, much more grounded steps in understanding the role of rotation in light phenomena were associated with development of the idea of light polarization [3]. The concept of elliptically polarized waves and the discovery of optical activity effects (Arago in 1811; Faraday in 1846 [4]) provided the rotational characteristics of light with a firm scientific background.

However, the real history of the problem begins from the famous Maxwell’s treatise [5] (1873), where the ideas of the electromagnetic field and its mechanical properties were first expressed in a clear and consistent form. Based on the Maxwell’s equations, Sadovsky [6] in 1898 and Poynting [7] in 1909 predicted that the light with a circular and elliptic polarization exerts the rotatory action upon

*Corresponding author at: o.angelsky@chnu.edu.ua

material objects, and a transparent analogy between a light beam with circular polarization and a rotating mechanical body was established. These ideas were supported in the careful experiments by Beth [8] in 1936 who managed to register the mechanical torque exerted by a circularly-polarized wave and, thereby, to determine the value of its angular momentum (AM).

Simultaneously, the electromagnetic theory made it possible to analyse energy flows associated with light waves. Probably, the first symptoms of a circulatory flow of light energy were discovered in 1919 during the theoretical study of focused optical fields [9]. The subsequent evolution of the classical and quantum field theory clearly indicated the existence of the photon spin and helicity, being the source of the spin angular momentum (SAM) of light associated with its non-planar polarization. On the other hand, consistent theoretical analyses of general light fields revealed numerous examples of the circulatory flows of light energy (see, e.g., Ref. 10) and even their ubiquity in the coherent irregular light fields, e.g., in speckle fields [11, 12]. Such structures were called “optical vortices” (OVs) [13]; to understand their fascinating mechanical features, the concept of an orbital angular momentum (OAM) previously developed in the pure-theoretical approach [14–16] was fruitfully employed.

But the real “boom” began in 1992 when Allen and his colleagues [17] calculated the AM of the well-known Laguerre-Gaussian modes of laser resonators and showed their remarkable similarity to circularly polarized beams. Since then, OVs have become perhaps the most popular objects of the modern optics. In particular, the OVs expose an important feature of all rotational effects: they are always accompanied by the presence of exceptional locations associated with the axis of rotation, where the field behaviour qualitatively differs from what can be seen at other (“generic”) points of space. Such exceptional points, termed as “optical singularities”, constitute another fruitful paradigm – “singular optics” [18–20] that have largely determined the optical science progress in the past decades.

The studies of singular points in spatial distributions of optical phase, polarization, amplitude, etc., laid a bridge to an extensive field of the wavefield topology, basically developed in the works of Nye, Berry, and their collaborators [21–23]. The specific properties of optical singularities, their characteristics and classification have shown that they form a coherent and interrelated system which determines the light field structure “as a whole”. Detailed analyses of optical singularities pave the way to the purposeful formation of light fields with a prescribed spatial, polarization, and spectral structures, and thus, contribute to the further development of the concept of “structured light”, attracting the special attention due to promising applications in optical manipulation, nano- and microengineering, data encoding, transmission, and processing [24–26].

Remarkably, various aspects of the physics and application of structured light demonstrate persuasive manifestations of the rotational and singular behaviour of light fields. Due to this circumstance, traditional instruments of the light characterization (distributions of amplitude, phase, polarization) become insufficient for

structured light fields. The dynamical characteristics (DCs) – spatial distributions of the energy, energy flow, momentum, angular momentum, and their derivatives – come to the fore, giving a consistent, informative, and application-oriented description [26–28].

An important feature of structured light fields is their principally 3D configuration: the usual representation of “transverse light waves” is no longer applicable [25, 27, 29]. The electric and magnetic vectors possess strong and variable longitudinal components, and this is the source of an additional sort of light rotation – “photonic wheels” [30, 31] where the light vectors rotate in the longitudinal plane. Upon proper employment, the longitudinal field components supply far-reaching prospects, in particular, for the near-field scanning optical microscopy; their engagement enables essential improvement in resolution and sensitivity of the optical diagnostic instruments up to nanometre scales. The DCs appear to be very useful in application to such fields, supplying meaningful and consistent concepts of transverse SAM and OAM [27, 32, 33].

Another useful toolbox for the structured light characterization, closely related to the DCs, is the system of its singularities. Each singularity appears as a topological object, and this topological nature makes the system of singularities stable against external perturbations. The singularities of different nature (singularities of phase, polarization, or energy flow, etc.) are interrelated; each singularity qualitatively “organizes” the field in its vicinity and enters certain harmonic relations with the adjacent singularities. In particular, the phase or polarization singularity stipulates a specific pattern of the field intensity, as well as the momentum and energy flow distribution around it. These interesting and informative patterns reflect deep physical regularities of the light fields, e.g. the interrelations between the spatial and polarization degrees of freedom [27, 32, 33]. In complex, the separate singularities form a coherent system (“singular skeleton” [34]) able to qualitatively represent the field as a whole, which can be used, in particular, for the reliable and economical optical data encoding and processing [25].

On the other hand, the optical singularities (as well as the patterns of DCs, by the way) are, generally, not immediately perceptible (sometimes they can be detected as the amplitude zeros, but in other cases this association can be elusive). As a rule, the singularities are detected indirectly via the interference with special “reference” waves of the simple standard structure [35–39], which puts no principal difficulties for the modern optical techniques. Anyway, the physical contents and technical possibilities associated with their wide use for the optical field inspection and characterization justify any effort directed to a deeper study of optical rotations and singularities.

Naturally, this interesting and vivid topic has been reviewed many times, with different degrees of generalization and with special attention to different fundamental and applied aspects. The full list of available reviews and compendia is too long; to name at least the most popular, at the authors’ discretion, Refs. 20, 34, 40–48 can be mentioned. In this record, each item contains a number of consistent references to original works, offered for readers intended to penetrate deeper into the corresponding sub-topics (e.g., nearly 500 titles in Ref. 47

treat the optical singularities in fibre waveguides; Ref. 48 cites over 600 publications on various features of the phase and polarization singularities, etc.).

In view of this background, an additional review can only be justified if it provides a new vision that was not sufficiently discussed previously. We hope this is the case. In this work, the authors systematically illustrate the rotational features of light fields and their associations with different sorts of optical singularities and their systems. On this basis, existing approaches to description and formation of the structured light fields, the role and manifestations of optical singularities are described, with the special attention to meaningful interrelations between different light-wave characteristics united by the singular networks.

2. Optical vortex: a prototype of optical singularities

2.1. General ideas and description

At the beginning, the general conventions relating to the terminology and notations that will be kept in the further presentation are outlined. The optical field is considered as an electromagnetic wave with space- and time-dependent electric $\mathbf{E}(\mathbf{R}, t)$ and magnetic $\mathbf{H}(\mathbf{R}, t)$ vectors, $\mathbf{R} = (x, y, z)^T$ is the 3D vector of spatial coordinates, and the superscript “ T ” denotes matrix transposition; t symbolizes time, as usual. As a rule, monochromatic fields are considered in which

$$\mathbf{E}(\mathbf{R}, t) = \text{Re}[\mathbf{E}(\mathbf{R}) \exp(-i\omega t)], \quad (1a)$$

$$\mathbf{H}(\mathbf{R}, t) = \text{Re}[\mathbf{H}(\mathbf{R}) \exp(-i\omega t)], \quad (1b)$$

where ω is the light frequency (polychromatic fields can always be considered as superpositions of monochromatic ones with different frequencies). The monochromatic fields are exhaustively characterized by the time-invariant complex quantities $\mathbf{E}(\mathbf{R})$, $\mathbf{H}(\mathbf{R})$. In regions without free charges and currents, the field vectors satisfy the Maxwell’s equations [49, 50]

$$\nabla \mathbf{H} = 0, \quad \mathbf{H} = \frac{1}{ik\mu} \nabla \times \mathbf{E}, \quad \nabla \mathbf{E} = 0, \quad \mathbf{E} = -\frac{1}{ik\varepsilon} \nabla \times \mathbf{H} \quad (2)$$

where $k = \omega/c$, c is the speed of light in vacuum, ε and μ are the permittivity and permeability of the medium, respectively, and the Gaussian system of units is used.

In many cases, the physically selected longitudinal direction z exists, and the rate of the field variations along z is much lower than that in the transverse (x, y) plane, and, in turn, the characteristic variations scale in the transverse plane is much higher than the vacuum wavelength $\lambda = 2\pi/k$. In such situations, the paraxial field model is appropriate where the electric and magnetic vectors are nearly transverse and described by equations

$$\mathbf{E} = \mathbf{E}_\perp + \mathbf{e}_z E_z = \left[\mathbf{u} + \frac{i}{kn} \mathbf{e}_z (\nabla_\perp \cdot \mathbf{u}) \right] e^{iknz}, \quad (3)$$

$$\begin{aligned} \mathbf{H} &= \mathbf{H}_\perp + \mathbf{e}_z H_z \\ &= \sqrt{\frac{\varepsilon}{\mu}} \left[(\mathbf{e}_z \times \mathbf{u}) + \frac{i}{kn} \mathbf{e}_z (\nabla_\perp \cdot (\mathbf{e}_z \times \mathbf{u})) \right] e^{iknz}. \end{aligned} \quad (4)$$

Here, the subscript “ \perp ” denotes the transverse part of the vector, $\mathbf{R}_\perp = \mathbf{r} = (x, y)^T$, \mathbf{e}_z is the unit vector of the longitudinal direction z , $n = \sqrt{\varepsilon\mu}$ is the medium refractive index, $\mathbf{u}(\mathbf{r}, z)$ is the paraxial complex amplitude [25, 27]

$$\mathbf{u} = \mathbf{e}_\perp u = \mathbf{e}_x u_x + \mathbf{e}_y u_y = \mathbf{e}_+ u_+ + \mathbf{e}_- u_-, \quad (5)$$

$\mathbf{e}_x, \mathbf{e}_y$ being the unit vectors of the transverse coordinates, and

$$\begin{aligned} \mathbf{e}_+ &= \frac{1}{\sqrt{2}} (\mathbf{e}_x + i\mathbf{e}_y), & \mathbf{e}_- &= \frac{1}{\sqrt{2}} (\mathbf{e}_x - i\mathbf{e}_y), \\ u_+ &= \frac{1}{\sqrt{2}} (u_x - iu_y), & u_- &= \frac{1}{\sqrt{2}} (u_x + iu_y) \end{aligned} \quad (6)$$

are the complex unit vectors and the transverse field components in the circular-polarization basis [27].

The transverse complex amplitude (5) satisfies the paraxial wave equation [27, 41]

$$i \frac{\partial u_\sigma}{\partial z} = -\frac{1}{2kn} \nabla_\perp^2 u_\sigma, \quad (7)$$

where $\nabla_\perp = \mathbf{e}_x \left(\frac{\partial}{\partial x} \right) + \mathbf{e}_y \left(\frac{\partial}{\partial y} \right)$ is the transverse gradient, whereas $\sigma = \pm 1$ for the basis of circular polarizations or $\sigma = x, y$ for the basis of linear polarization, which are equally admissible in the paraxial approximation. The main (first) terms of (3) and (4) describe the transverse field components, while the longitudinal components (second terms) are of the relative order $\gamma = (kb)^{-1}$ in magnitude, with b being the characteristic transverse scale of the distribution $\mathbf{u}(\mathbf{r}, z)$. The quantity γ is the small parameter of the paraxial approximation; the longitudinal characteristic scale of the paraxial beam equals $z_R = kb^2$.

The main DC of an optical field is its energy density averaged over the period of oscillations [27, 32, 49]

$$\begin{aligned} w &= w^e + w^m = \frac{g}{2} (\varepsilon |\mathbf{E}|^2 + \mu |\mathbf{H}|^2) = g\varepsilon (\mathbf{u}^* \cdot \mathbf{u}) \\ &= g\varepsilon (|u_x|^2 + |u_y|^2), \end{aligned} \quad (8)$$

whereas the energy flow density is given by the time-averaged Poynting vector [25, 27, 49]

$$\mathbf{S} = \frac{c^2}{n^2} \mathbf{p} = cg \text{Re}[\mathbf{E}^* \times \mathbf{H}] \quad (9)$$

($g = (8\pi)^{-1}$ in the Gaussian system of units). Here \mathbf{p} is the field momentum density, according to [25] taken in the Minkowski form. It can be decomposed into the sum of the “orbital” \mathbf{p}^O and “spin” \mathbf{p}^S momenta expressing the roles of the spatial and polarization degrees of freedom [25, 27, 32, 51],

$$\mathbf{p} = \mathbf{p}^O + \mathbf{p}^S \quad (10)$$

where

$$\mathbf{p}^O = \frac{g}{2\omega} \text{Im}[\varepsilon \mathbf{E}^* \cdot (\nabla) \mathbf{E} + \mu \mathbf{H}^* \cdot (\nabla) \mathbf{H}], \quad (11)$$

$$\mathbf{p}^S = \frac{g}{4\omega} \text{Im}[\nabla \times (\varepsilon \mathbf{E}^* \times \mathbf{E} + \mu \mathbf{H}^* \times \mathbf{H})]. \quad (12)$$

For the paraxial field of (3) and (4), the momentum density can be suitably presented in the form

$$\mathbf{p} = \mathbf{p}_{\parallel}^o + \mathbf{p}_{\perp}^o + \mathbf{p}_{\perp}^s, \quad (13)$$

where the longitudinal component

$$\mathbf{p}_{\parallel}^o = \frac{g}{c} \varepsilon n \mathbf{e}_z (\mathbf{u}^* \cdot \mathbf{u}) = \frac{n}{c} w \mathbf{e}_z \quad (14)$$

describes the main (longitudinal) energy flow and momentum whereas the transverse momentum containing the orbital and spin parts,

$$\begin{aligned} \mathbf{p}_{\perp}^o &= \frac{g}{ck} \varepsilon \operatorname{Im}(\mathbf{u}^* \cdot (\nabla_{\perp} \mathbf{u})) \\ &= \frac{g}{\omega} \varepsilon (|u_+|^2 \nabla_{\perp} \varphi_+ + |u_-|^2 \nabla_{\perp} \varphi_-), \end{aligned} \quad (15)$$

$$\begin{aligned} \mathbf{p}_{\perp}^s &= -\frac{i}{2\omega} g \varepsilon (\nabla_{\perp} \cdot [\mathbf{u}^* \times \mathbf{u}]) \\ &= \varepsilon \frac{g}{2\omega} \left(\mathbf{e}_x \frac{\partial}{\partial y} - \mathbf{e}_y \frac{\partial}{\partial x} \right) (|u_+|^2 - |u_-|^2) \end{aligned} \quad (16)$$

express the intrinsic structure of the field, including its rotational features. For example, the OAM and SAM densities with respect to the beam axis are determined from (15) and (16) as

$$\begin{aligned} \mathbf{L} &= \mathbf{r} \times \mathbf{p}_{\perp}^o = \mathbf{e}_z L_z = \mathbf{e}_z \frac{g}{\omega} \varepsilon \\ &\quad \times \left[|u_+|^2 \left(x \frac{\partial \varphi_+}{\partial y} - y \frac{\partial \varphi_+}{\partial x} \right) + |u_-|^2 \left(x \frac{\partial \varphi_-}{\partial y} - y \frac{\partial \varphi_-}{\partial x} \right) \right] \\ &= \mathbf{e}_z \frac{g}{\omega} \varepsilon \left[|u_+|^2 \frac{\partial \varphi_+(\mathbf{r})}{\partial \phi} + |u_-|^2 \frac{\partial \varphi_-(\mathbf{r})}{\partial \phi} \right], \\ \mathbf{s} &= \mathbf{r} \times \mathbf{p}_{\perp}^s = \mathbf{e}_z s_z \\ &= -\mathbf{e}_z \frac{g}{2\omega} \varepsilon \left(x \frac{\partial}{\partial x} + y \frac{\partial}{\partial y} \right) (|u_+|^2 - |u_-|^2). \end{aligned} \quad (18)$$

Particularly, in case of linear polarization, when $|u_+(\mathbf{r})| = |u_-(\mathbf{r})|$ and the phases $\varphi_+(\mathbf{r})$, $\varphi_-(\mathbf{r})$ differ only by a constant, the OAM density expression (17) gives, generally, a meaningful non-zero result while the SAM (18) expectedly vanishes. The total values of the DCs for

the “whole beam” per unit z -length are characterized by the “integral” quantities:

$$\begin{aligned} \langle w \rangle &= \int w(\mathbf{r}) d^2 \mathbf{r}, \quad \langle \mathbf{p} \rangle = \int \mathbf{p}(\mathbf{r}) d^2 \mathbf{r}, \\ \langle \mathbf{L} \rangle &= \int \mathbf{L}(\mathbf{r}) d^2 \mathbf{r}, \quad \langle \mathbf{s} \rangle = \int \mathbf{s}(\mathbf{r}) d^2 \mathbf{r}; \end{aligned} \quad (19)$$

note that the integration by parts in the latter equation shows [27, 41] that, for any spatially-limited field, the SAM density representation (18) is equivalent to the usual form

$$\mathbf{s} = \mathbf{e}_z \frac{g}{\omega} \varepsilon (|u_+|^2 - |u_-|^2). \quad (20)$$

2.2. Structure of optical vortices

OVs frequently occur in various optical fields [20], but “generically” are associated with paraxial fields, and are suitably considered within the frame of the above-described paraxial approximation (3)–(7). As a rule, an OV appears in a single polarization component and can thus be treated as the “scalar singularity” [20, 27, 41] which can exist independently of the beam polarization. Its geometrical structure and main attributes are typical to many other optical singularities, so in this section, the OV parameters are considered in more detail.

In a circular OV, the scalar complex amplitude (7) is characterized by the “helical phase factor”

$$u(\mathbf{r}, z) = f(r, z) \exp(il\phi), \quad (21)$$

where $\phi = \arctan(y/x)$ and r are the polar coordinates in the beam cross section. According to (21), on a round-trip near the longitudinal axis z , the field phase does not return to its initial value but experiences an increment $2l\pi$, which corresponds to the helical wavefront shape [screw wavefront dislocation [18], see Fig. 1(a)]; this means that the phase is indeterminate (singular) in the point $(x=0, y=0)$. These properties are compatible with the field definiteness (and with the smooth, unambiguous solutions of the Maxwell’s equations) only if l is an integer number called “topological charge” (TC), and the field

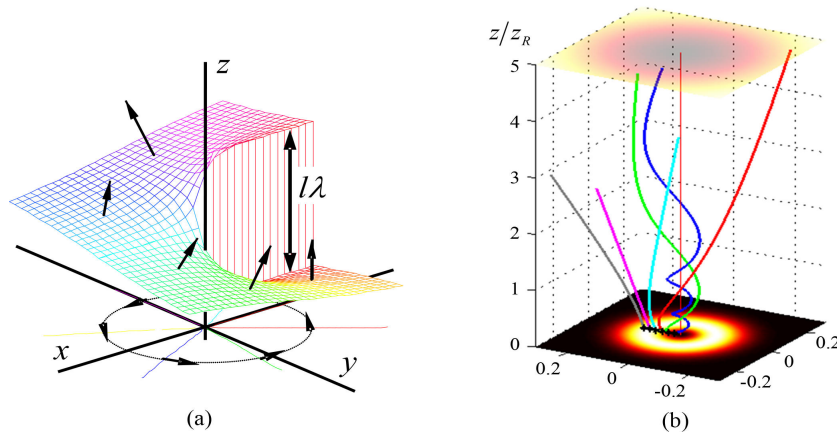


Fig. 1. (a) Wavefront of an OV beam near the OV core: normals to the screw-like surface are inclined with respect to the longitudinal direction; their azimuthal components form a close-loop circulation in the beam cross section. (b) 3D lines of the energy propagation in a circular OV beam for different distances from the beam axis in the waist plane $z = 0$.

amplitude distribution possesses an isolated zero point (the OV core) at the screw axis. Accordingly, the intensity distribution forms a bright ring [Fig. 1(b)]. Local directions of the energy flows are normal to the wavefront [27, 52], and due to its helical shape, each wavefront normal possesses a certain azimuthal component; altogether, these azimuthal components form a closed loop in the transverse cross section [Fig. 1(a)]. This makes the energy propagate along complicated spiral lines [Fig. 1(b)] rather than along the longitudinal rays as is typical for usual optical fields. The transverse components of the energy flow are responsible for the transverse energy circulation which is a characteristic feature of the OV field and a source of the mechanical angular momentum, namely, OAM carried by the OV.

The circularly symmetric pattern depicted in Fig. 1 shows an ideal configuration typical for circular OV beams (the well-known standard OV models using the Laguerre-Gaussian (LG), Bessel, Kummer beams, etc. [20, 27, 41, 53–56]). The LG beams are generally considered as standard scalar OV-beam models with the complex amplitude distribution of (21) where

$$\begin{aligned}
 f(r, z) &\equiv f_{LG}(r, z) \\
 &= E_0 \sqrt{\frac{|l|!}{(p + |l|)! b(z)}} \left(\frac{r}{b(z)}\right)^{|l|} L_p^{|l|} \left(\frac{r^2}{b^2(z)}\right) \exp\left(-\frac{r^2}{b^2(z)}\right) \\
 &\quad \times \exp\left[i\left(kz + \frac{kr^2}{2R(z)} - \chi(z)\right)\right]. \quad (22)
 \end{aligned}$$

In this equation,

$$\begin{aligned}
 b^2(z) &= b_0^2 \left(1 + \frac{z^2}{z_R^2}\right), \quad R(z) = \frac{z^2 + z_R^2}{z} \\
 \chi(z) &= (2p + |l| + 1) \arctan\left(\frac{z}{z_R}\right)
 \end{aligned}$$

are the z -dependent beam radius, the wavefront radius of curvature, and the so called Gouy phase [20], correspondingly; $L_p^{|l|}(\dots)$ is the Laguerre polynomial [57], integer $p > 0$ is the radial index and the TC l coincides with the azimuthal index of the LG mode. Here b_0 denotes the minimum beam radius at the “waist plane” where the longitudinal coordinate $z = 0$; the Rayleigh length $z_R = kb_0^2$ specifies the longitudinal scale of the field, corresponding to z_R below (7). Remarkably, the OAM of such a beam (per unit z -length) with allowance for (17) and (19) equals to [17, 58]

$$\langle L_z \rangle = l \frac{\langle w \rangle}{\omega}. \quad (23)$$

Accordingly, each photon with the energy $w^{\text{ph}} = \hbar\omega$ carries the OAM $L_z^{\text{ph}} = l\hbar$ [17] (just like a circularly polarized photon carries the SAM $s_z^{\text{ph}} = \sigma\hbar$ where $\sigma = \pm 1$ is the quantum number of circular polarization). The LG mode (21), (22) is characterized by the ring-like intensity distribution with $p + 1$ bright rings; since the OAM depends only on l , in most applications the zero-index LG_0^l beams are preferable with the one-ring (“doughnut”) intensity pattern [cf. Fig. 1(b)].

In many real situations this ideal pattern is distorted; moreover, a minor symmetry-breaking perturbation destroys a multicharged OV (21) (with $|l| > 1$) into a set of $|l|$ separate single-charged ones [20, 27, 41]. However, even in asymmetric situations, just near the core (supposed to be situated at the point $x = x_V, y = y_V$ of the beam cross section), the complex amplitude distribution can be described in a universal way as

$$\begin{aligned}
 u(\mathbf{r}) &\approx \beta_x(x - x_V) + i\beta_y(y - y_V) \\
 &= \sqrt{|\beta_x|^2(x - x_V)^2 + |\beta_y|^2(y - y_V)^2 + 2\text{Im}(\beta_x\beta_y^*)(x - x_V)(y - y_V)} \\
 &\quad \times \exp\left(i \arctan \frac{\text{Im} \beta_x(x - x_V) + \text{Re} \beta_y(y - y_V)}{\text{Re} \beta_x(x - x_V) + \text{Im} \beta_y(y - y_V)}\right), \quad (24)
 \end{aligned}$$

where β_x and β_y are the complex parameters determining the OV morphology [41, 59, 60]. In contrast to the circular OV (21), this structure is asymmetric (“anisotropic OV”): the equal-amplitude lines are ellipses, the rate of the phase change upon the near-OV circulation is non-uniform. Under external influences (e.g., the beam propagation through inhomogeneous medium), parameters of (24) $\beta_x, \beta_y, x_V, y_V$ may change but the singularity ‘per se’ with all its attributes (isolated amplitude zero, screw wavefront dislocation, transverse energy circulation) is of the topological nature and, therefore, stable against perturbations. For this reason, OV beams are promising for the information transfer in noise conditions, e.g., through the turbulent atmosphere [24].

2.3. Interference properties and generation of optical vortices

The most impressive features of the OV beams are demonstrated when they interfere with non-singular waves possessing smooth wavefronts. Upon the coaxial interference, the wavefront helicity leads to the spiral fringes [Fig. 2(a)] which transform into the characteristic “broken” lines and the “fork” structure [Fig. 2(b)] with a growing angle between the LG beam and the reference wave axes. The interference patterns with “broken” fringes and “forks” still remain the most suitable indicator of the OV widely used for their detection [19, 20, 35–39, 41]. Remarkably, the fork orientation (“up” or “down”) allows to distinguish positive or negative TCs l .

On the other hand, the interference patterns obtained with the OV beams open the most flexible and universal ways for generating such beams in practice. First

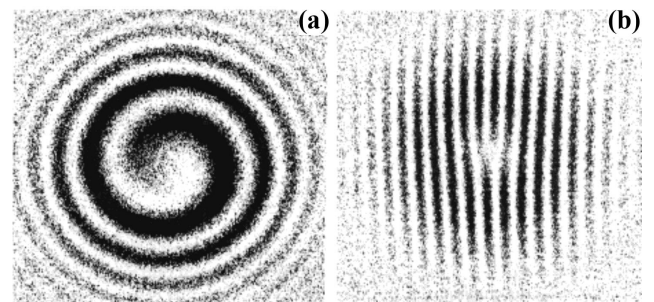


Fig. 2. Patterns of interference between the circular LG mode (22) with $|l| = 1$ and the plane wave: (a) when both waves are coaxial and (b) when the waves are mutually inclined.

observations dealt with occasional OV's emerging in the speckle fields [61] and/or with the LG modes of laser resonators that can be realized upon proper distribution of losses over the resonator cross section with axial maximum. The generation of a beam with OV immediately inside the laser cavity is, probably, the simplest method for the purposeful OV generation. Simultaneously, this method is the least reliable because the conditions necessary for the LG mode formation may be unfavourable for the laser generation 'per se' (that is why an easier version of the "in-cavity" OV beam creation employs the more usual laser-generated Hermite-Gaussian modes, from which the OV beam can be obtained by means of properly adjusted astigmatic mode converters [62, 63]).

As is well known [64], if some recording medium carries the pattern of interference between an arbitrary "object" beam and a standard "reference" beam, then, after illuminating this structure with a more or less accurate copy of the reference beam, the object beam structure can be restored in the diffracted field. In application to OV, this approach was first realized even before the "singular" era [18] and obtained further development, with many modifications and technical improvements, in a lot of subsequent works [38, 53, 60, 65–68]. The necessary interference pattern, based on the desired OV-beam structure, can be calculated and afterwards reproduced in the optical transparency or, more flexibly, with the programmable spatial light modulator [39–42]. Examples of the OV-producing gratings ("computer-generated holograms" [20]) are presented in Fig. 3. It can be seen that at the periphery they look like ordinary diffraction gratings with rectilinear grooves but contain the groove bifurcation ("fork" structure) in the central area, which is responsible for the OV formation.

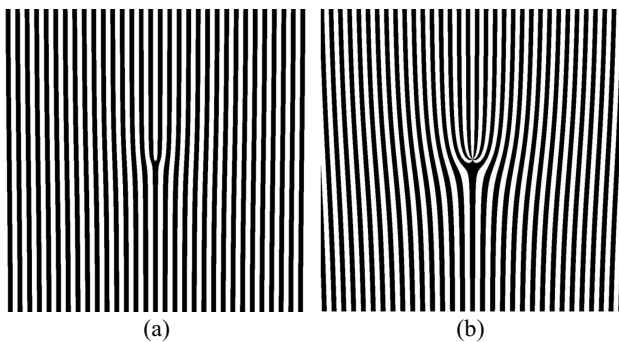


Fig. 3. Examples of the gratings designed for the OV generation: (a) with the TC $|l| = 1$; (b) with the TC $|l| = 5$.

If the incident Gaussian beam diffracts on a structure depicted in Fig. 3(a), the zero-order (non-diffracted) beam still remains Gaussian, but in the $\pm N$ th diffraction order, the OV beam with the TC $l = \pm N$ is formed. In contrast, the grating of Fig. 3(b) in the $\pm N$ th diffraction order produces the OV beam with the TC $l = \pm 5N$. It should be noted that the OV beams formed by such gratings from the incident Gaussian beams do not belong to the LG family; the groove bifurcation introduces a "sharp" complex amplitude discontinuity due to which the beam amplitude decays as $\sim r^{-2}$ with the growing transverse radius r , instead of the exponential decay in the LG beams (22). For this reason, the OV beams formed by the "fork" gratings have no second-order intensity moments [69], i.e., their

"weighted" width tends to infinity (like in Bessel beams or sharp-edge diffracted beams [70]); they form a special class of Kummer, or hypergeometric-Gaussian, beams [53, 54, 56, 57]. As far as the angle of diffraction is small, the Kummer beams possess a circular symmetry, but at high diffraction angles this symmetry is broken [60].

The same circular Kummer beams can be obtained when a Gaussian beam passes the special phase plate with helical relief (spiral phase plate) which imparts the phase retardation corresponding to the helical wavefront of Fig. 1(a) [71–73]. There are many other methods for the OV generation, but those are less popular due to the need for the special light polarization and anisotropic or liquid-crystal elements [74–77].

Note that all methods performing the controllable spatially-dependent phase retardation are, in principle, able to realize the phase multiplier in (21) with the arbitrary l , including non-integer. In the latter case, the so called "fractional OV" can be generated [78]. However, the wave in the form (21) with the fractional l is not a solution of the Maxwell's equations (2) and thus can only be realized in a single cross section; upon further propagation, the "fractional OV" transforms into a complicated asymmetric complex-amplitude distribution containing a series of oppositely-signed single-charge vortices [72, 79].

2.4. Rotational Doppler effect

Generally, optical fields contain a system of singularities which coexist, interact, and obey certain common principles of the structured light organization [80, 81] (see for example Fig. 4). These principles follow from the topological "unity" of the beam: all the wavefront dislocations should be compatible with the wavefront continuity and connectivity in all other points; similarly, the transverse energy flows near each OV core should be compatible with the continuity and connectivity of the "global" energy flow pattern. In other words, the rotational properties of such generic fields are manifested in small scales but, as a rule, are not characteristic for the beam as a whole. In contrast, the standard OV models (for which the LG mode (22) is a typical example) demonstrate the singular and rotational properties explicitly, as the attributes of the beam 'per se'.

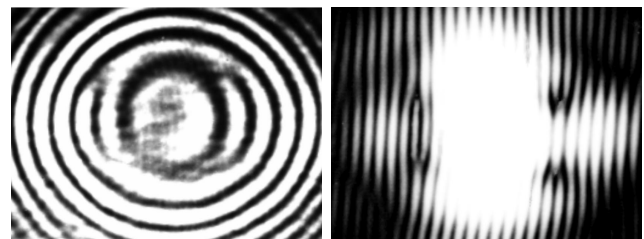


Fig. 4. Formation of the four OV's ("quadrupole") upon the beam propagation through the light-induced non-linear astigmatic lens [19].

Here, one of such interesting rotational qualities of the circular OV beams – the rotational Doppler effect (RDE) is briefly considered. Previously, it was revealed and elaborated for the circularly-polarized beams [82–86], but the circular OV beams possess this property as well. The RDE originates from the beam phase dependence on the azimuth angle (21). Accordingly, the phase "seen" by an

observer “peering” against the z -axis [Fig. 5(a)] depends on its azimuthal orientation, and the OV beam observable frequency depends on the mutual mechanical rotation of the beam and observer about the beam axis [87–92]. On the other hand, the RDE can be treated via the change of the circular vortex photon energy $\hbar\omega$ due to the work performed by the optical elements implementing rotation of the beam with OAM (this way of reasoning represents a dynamic approach to deformations of optical systems: any such deformation is accompanied by the mechanical work performed by the optical forces, which changes the energy of the light wave circulating in the system [93–96]). If the beam’s TC is l , and, accordingly, the OAM is determined by (23), its rotation with the angular velocity Ω changes the energy of each photon by $\Delta(\hbar\omega) = \hbar l\Omega$, which is equivalent to the frequency shift $l\Omega$.

At first glance, the RDE concept is specific to circular beams with OAM and cannot be applied to other light fields. But due to the completeness of the system of LG modes [57], an arbitrary optical field can be represented as a superposition of circular LG beams with different radial p and azimuthal l indices [20, 41]. The rotation of such a field means that its individual LG components experience the RDE frequency shifts, i.e., due to rotation of a monochromatic beam, a superposition of fields with different frequencies appears. Such a superposition cannot be stationary: the beats emerge at the “side” frequencies equal to the frequency differences of the LG components, and a variable signal can be registered by any photodetector. On the other hand, this variable signal can be considered as a purely geometric effect due to the rotation: the inhomogeneous beam profile moves across the fixed photodetector aperture, and the latter registers a variable signal [41].

Therefore, arbitrary rotation of an optical field (for example, rotation of an image) can be interpreted as the RDE of its LG components, and the analysis of the variable signal that occurs in a spatially fixed detector allows to investigate the composition of the corresponding LG-modes superposition (the LG spectrum) [97]. On this basis, effective methods for detecting and studying the RDE through a visible rotation of the intensity profile of a certain superposition of the vortex and non-vortex beams can be constructed [89–91].

Naturally, interpretation of the visible motion of an image as interference between its components with different Doppler frequency shifts is possible not only in

the case of RDE but also for the usual “linear” Doppler effect. In this case, the transverse translational motion of the field leads to changes in the frequencies of its angular Fourier components (plane waves), and the analysis of the variable signal can give information about the spatial Fourier spectrum (plane-wave spectrum) of the field [41].

The dynamic approach to RDE proved to be especially useful in application to specific phenomena that occur when the beam rotates around an axis that differs from the beam axis [“non-collinear RDE” [41, 92], Fig. 5(b)]. Calculation of the work of the optical forces expended on the rotation of the “inclined” LG beam gives $-2l\hbar\Omega \cos^2 \beta$ “per photon”, from which the frequency shift $\Delta\omega = -2l\Omega \cos^2 \beta$ seemingly follows. This result looks quite understandable, but it entails rather strange consequences. First, after a complete revolution, when the system of Fig. 5(b) returns to its initial state, the phase increment is not a multiple of 2π . Moreover, accounting for the unambiguous relationship between the phase and the angle of rotation of the LG beam, such an increase in phase means that the beam does not return to its original position – in sharp contrast to the common sense and everyday experience. The paradox becomes especially obvious when the two cases of a conical scan [Fig. 5(b)] are compared. If the input beam carries a certain image, then when reflected “forward”, which takes place if the mirror is tilted by $\beta < 45^\circ$, this image rotates twice on each full rotation of the mirror, and when reflected “backward” ($\beta > 45^\circ$), the original image does not rotate at all. From the first situation to the second one, it is possible to pass continuously, changing the mirror inclination; but in any case, one can see only an integer number of revolutions of the image on one cycle of mirror rotation, and a continuous transition from “two revolutions” to “no revolutions” cannot be imagined.

The key to solving these puzzles is to carefully analyse the conditions for observing these frequency shifts and image rotations. In this situation, as nowhere else, the specific connection of the observed phase or frequency of the OV beam with the relative position of the beam and the recording system (observer) is clearly revealed. It turns out that not all reference systems are equal: there must be a “privileged” frame in which the behaviour of the beam during conical scanning looks the most “natural”. The analysis shows [92] that such a frame can be represented as a Cartesian (X, Y) -plane, orthogonal to the moving axis of

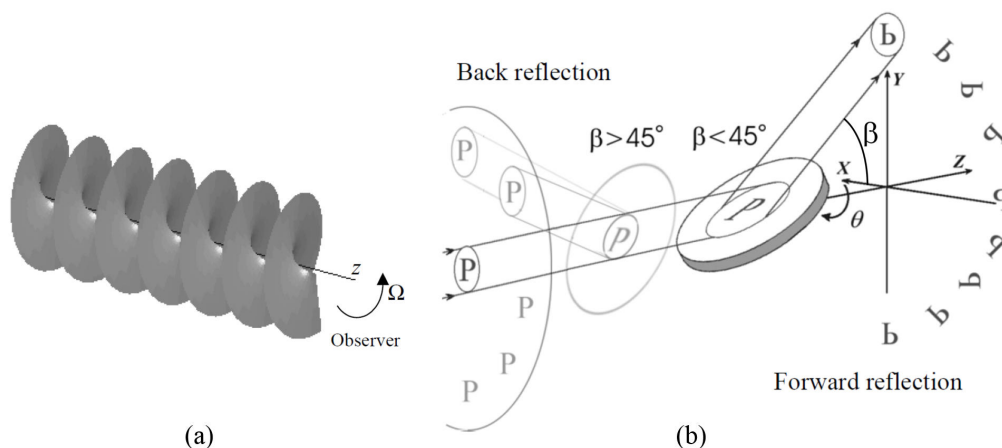


Fig. 5. Illustration of the RDE: (a) usual scheme, (b) non-collinear RDE with the beam conical evolution.

the beam in Fig. 5(b), and at each moment of motion the angle between the X -axis and the circular trajectory of the beam axis is $\Delta\alpha = \Delta\theta \cos 2\beta$. Taking this motion of the reference frame into account, all the above-mentioned paradoxes of non-collinear RDE find their solutions [92].

The described phenomena have a purely geometric nature and appear due to peculiarities of the composition of rotational motions with respect to different non-collinear axes (for example, Rytov’s law for the rotation of the polarization plane of a twisted beam of light, or the motion of the Foucault pendulum [98], etc.). They are manifestations of the Berry topological phase, inherent in the evolution of nonholonomic systems. The topological nature of these effects makes them insensitive to a particular path of evolution; similar “non-integer” phase shift and rotation of the reference frame will occur when the axis of the output beam does not follow the cone surface, as in Fig. 5(b), but describes a closed loop of any shape. Additional phase and additional rotational displacement of the beam are also manifestations of the geometric phase which, however, are visible only to the “natural” observer. In a laboratory system, the geometric phases associated with the motion of the reference frame and with the motion of the beam with respect to this frame are completely compensated and, therefore, none of them is directly observed.

2.5. Mechanical properties of circular light beams

Consistent application of the DC-based formalism to the OV beams enables to disclose their interesting, non-trivial mechanical features [99]. A circular OV beam can be likened to a rotating mechanical body. Considering an OV beam as a mechanical body, its mechanical characteristics such as the angular velocity can be introduced, which for the LG beam (22) is naturally defined as [99]

$$\Omega(z) = \frac{c}{kb^2(z)} = \frac{\omega}{k^2b^2(z)} \quad (25)$$

(this expression is derived from observation of the visible rotation of slightly asymmetric perturbed LG beams during their propagation; note that it does not include the TC l , and, since in the paraxial limit $kb \gg 1$, Ω is much less than the optical frequency ω). The corresponding mass [more accurately, the linear mass density defined according to the rule (19)] is determined by the electromagnetic mass of the light field, $m_e = \langle w \rangle / c^2$. Then, the beam OAM can be written in the “body-like” form

$$\langle L_z \rangle = J(z)\Omega(z), \quad (26)$$

which is compatible with (23) and (25) if

$$J(z) = lm_e b^2(z). \quad (27)$$

The quantity $J(z)$ has a meaning of the moment of inertia per unit length of the beam. Its expression appears to be very similar to the known expression $J(z) = 2m_e b^2(z)$ for the moment of inertia of an inhomogeneous mechanical body [41] in which the radial mass distribution is the same as in the LG_0^l beam; the only difference is the additional coefficient 2. This difference is caused by the fact that in

the “body”, modelling a vortex beam, the OAM density is proportional to the intensity, that is, to the electromagnetic mass distribution while in a rigid body, the points remote from the axis produce greater contributions since their velocities are proportional to the off-axis distances. The proportionality between the OAM and the electromagnetic mass distributions can be explained only by supposing that, in the mechanical model of an LG beam, the linear velocities of different radial layers do not grow with their off-axial distances but, oppositely, decrease with inverse proportionality to the radius r [99]. Remarkably, such a distribution of the velocities of the layers rotation is typical for other physical vortices (in a liquid, in the atmosphere, etc. [41]), which convincingly testifies to the unity of the physical laws of the world and additionally justifies the term “optical vortex”.

Based on (25)–(27), the kinetic energy (per unit length) associated with the LG-beam rotation can be derived:

$$W_k = \frac{1}{2}J(z)\Omega^2(z) = \frac{l}{2} \frac{\langle w \rangle}{k^2 b^2(z)} \quad (28)$$

Noticeably, this quantity, as well as the velocity (25), rapidly grows with the beam squeezing (e.g., due to focusing). Indeed, when the beam radius decreases, its energy is concentrated closely to the axis where, according to Fig. 1(a), the wavefront normals are inclined more strongly, and the azimuthal components of the Poynting vector grow correspondingly [100]. It can be formulated that the focusing elements perform a mechanical work accelerating the OV beam rotation and increasing its mechanical energy (28); however, the intrinsic energy of the beam $\langle w \rangle$ remains unchanged.

It is reasonable to mention another mechanical model of a circular OV beam (21), directly addressing its helical symmetry [99]. First, it is supposed that the pre-exponential function $f(r, z) \simeq f(r)$ does not depend on z , or this dependence is negligible (which is correct near the beam waist). Then, the beam (21) is a pure-helical object whose translation along the axis z with the speed of light c is equivalent to the rotation around the same axis with the angular velocity ω/l ; actually, these are not two different motions but rather the same motion can be treated in two ways. Thus, its kinetic energy can be ascribed either to the rotation or to the translational motion, which, in application to the unit z -length of the beam and with involvement of the corresponding mass m_e [see (27)] and the electromagnetic moment of inertia J_e (as yet unknown) yields

$$\frac{1}{2}J_e \left(\frac{\omega}{l}\right)^2 = \frac{1}{2}m_e c^2. \quad (29)$$

Hence, the expression for J_e immediately follows,

$$J_e = m_e c^2 \left(\frac{l}{\omega}\right)^2 = \langle w \rangle \left(\frac{l}{\omega}\right)^2. \quad (30)$$

This final result does not depend on the mass m_e definition and can be considered as a universal law for objects with this sort of symmetry. By the way, it determines the electromagnetic AM per unit beam length as $L_e = J_e(\omega/l) = l \frac{\langle w \rangle}{\omega}$ which exactly coincides with (23)

obtained via the direct calculation of the OAM from the definitions (17), (19) and using the beam model (22). As one can see, the relationship (23) between the helical beam energy and its OAM obtains substantiation in the helical symmetry alone and can, thus, be considered a universal property of all propagating light fields with the helical symmetry type.

To finalize the presentation of mechanical features of circular OV beams (21), it is important to emphasize yet another interesting kinematic property [20]. In “scalar” paraxial fields, the transverse part of the instantaneous field vector (1a) can be represented as $\mathbf{E}_\perp(\mathbf{R}, t) = \mathbf{e}_\perp \text{Re}[u(\mathbf{R})e^{-i\omega t}] = \mathbf{e}_\perp E(\mathbf{R}, t)$ [see (3) and (5)]. Applying this for the OV field (21), one obtains the instantaneous scalar field value $E(\mathbf{R}, t) = E(x, y, z, t)$ in the form

$$E(r, \phi, z, t) = \text{Re}[f(r, z)] \cos(kz + l\phi - \omega t) - \text{Im}[f(r, z)] \sin(kz + l\phi - \omega t), \quad (31)$$

which testifies that in a fixed cross section ($z = \text{const}$) the instantaneous field depends on $l\phi - \omega t$, i.e., rotates with the angular velocity $d\phi/dt = \omega/l$ (in contrast to the “usual” fields with no azimuthal phase dependence which simply oscillate in each point). This property remarkably underlines the rotational nature of the OV beams; however, it has no direct mechanical meaning because it dictates that at points with $r > l/k$, the linear velocity of rotation exceeds c , which is inappropriate for any mechanical model.

The fact of the instantaneous field rotation in the circular OV beams stimulated the search for similar instantaneous motions in other beams with OAM. Generally, the pattern of instantaneous oscillations in beams of general form is rather complicated, and the presence of the rotating component of instantaneous oscillations is not obvious. But it can be detected due to correlations between the time and azimuthal derivatives of the instantaneous electric field distribution:

$$\left\langle \frac{\partial E(x, y, t)}{\partial t} \frac{\partial E(x, y, t)}{\partial \phi} \right\rangle_T, \quad (32)$$

where $\langle \dots \rangle_T$ means averaging over the oscillation period. The corresponding analysis has shown [27, 101] that for any scalar paraxial field $E(x, y, t)$, the quantity (32) is proportional to the OAM. Therefore, the rotational properties of light beams at the observable time scale are immediately related with the rotational motion of the instant field-oscillation pattern, and the OAM is just the natural kinematic measure of this rotational motion.

Note by the way that this property is not an exclusive attribute of the rotational fields. It was shown in the subsequent studies [102] that any directional motion that can be identified in the pattern of instantaneous oscillations means the presence of a directed energy flow in the experimentally observable time-averaged field. In this case, the orbital momentum density (15) acts as a natural geometric and kinematic characteristic of the “directed” component of the instantaneous oscillations. In fact, this is a generalization of the well-known picture of a traveling plane wave, but in complex fields the “running” component of the instantaneous oscillations is often elusive and can

thus be detected only through the correlation analysis, which leads to the density of an “average” energy flow proportional to the orbital momentum. This conclusion very spectacularly reveals the immediate physical causes and hidden mechanisms of formation of the directed energy flows in light fields [27]. However, it is only applicable to “scalar” fields whose polarization is homogeneous, or to the “partial” fields of separate linearly polarized components of general vector fields (see section 5 below). In vector beams, the instantaneous “running” patterns of separate polarization components may mutually cancel out so that for the whole field, the instantaneous energy and momentum distributions do not depend on time (“steady” beams [103–105]).

Importantly, it is the orbital momentum (11) [more accurately, its transverse part (15)] that is a characteristic of the running pattern of instantaneous oscillations. The spin part (16) of the transverse momentum density, on the contrary, cannot be associated with any spatial motion of the instantaneous field picture. This is due to the special role of the polarization degrees of freedom associated with the “invisible” rotational motion of the field vectors in the “abstract” polarization space. This difference is an additional important feature that reflects a deep physical discrepancy between the orbital (11) and spin (12) momentum contributions.

The intriguing dynamical properties of the OV fields described in this section are especially attractive for optical manipulation techniques [106–118] performing the mechanical action on particles suspended inside the field of strongly focused singular beam. As an isolated zero of intensity, the OV core acts as an axial optical trap for absorbing, reflective or low-index particles [106–111]; dielectric particles with refractive index higher than that of environment can be trapped off-axially inside the bright ring [112]. In contrast to the usual optical trapping at the intensity maxima, trapping in the low-intensity area of the OV core provides certain advantages, e.g., for the study of biological objects sensitive to laser radiation [116–118].

In all cases of trapping with OV beams, trapped objects interact with the beam OAM, which enables to perform their controllable rotation and orientation: “optical spanners” and “optically driven micromachines” can be realized [113–118]. The beams with several OVs, that form coherent networks of singularities, offer additional impressive possibilities in optical manipulation of multiple particles [119–121]; it is especially suitable that the positions and morphologies of the separate OVs can be easily regulated, e.g., by changing the interfering fields intensities, with no direct contact and no movable parts of the optical system. In general, the optical manipulation is one of the main fields for the singular-optics applications with the rapidly developing techniques and ideas.

3. Methods for generation of optical singularities

In section 2.3, the most common method for obtaining OVs using synthesized holograms was considered. Despite that it was developed in the 90s [35–40, 100, 122–124], the similar approaches are still in charge in many fundamental and applied works. However, the further application of such methods is prohibited by one significant drawback, namely, relatively low energy efficiency, which is a

consequence of the beam energy loss during the diffraction on the hologram. That is why even now there is a need to develop alternative methods for generating singularities of different types.

3.1. Generation of wavefront dislocations

Following to [39, 122, 123], one can consider the interference of two waves with complex amplitudes

$$u_1(x, y) = A_1(x, y) \exp[i\Phi_1(x, y)]; \quad (33a)$$

$$u_2(x, y) = A_2(x, y) \exp[i\Phi_2(x, y)] \quad (33b)$$

and suppose that in the region of interest the waves parameters do not change (the self-diffraction transformations are negligible). In the point (x, y) of the observation plane, the wave amplitudes differ insubstantially, and the solution of equation $A_1(x, y) = A_2(x, y)$ exists in the form $y = f(x)$ – a line of equal intensities of the waves. The condition for an isolated zero of the combined field $u_1(x, y) + u_2(x, y)$ can be written in the form

$$\begin{cases} \Phi_1(x_i, y_i) = \Phi_2(x_i, y_i) + \pi = \Phi_i, \\ A_1(x_i, y_i) = A_2(x_i, y_i) = A_i, \end{cases} \quad (34)$$

where x_i, y_i are the transverse coordinates of the i -th zero of amplitude. In the local frame X, Y with the origin in the point (x_i, y_i) , the phase of the sum field (phase of the OV) is determined by

$$\tan \Phi = A_i \frac{\Delta\Phi_i^x X + \Delta\Phi_i^y Y}{\Delta A_i^x X + \Delta A_i^y Y}, \quad (35)$$

where $\Delta\Phi_i^x, \Delta\Phi_i^y, \Delta A_i^x$ and ΔA_i^y are the (X, Y) components of the gradients of the quantities Φ_i and A_i . This means that the resulting-field phase (and, accordingly, the sign of the TC) is completely determined by the phase gradients and amplitudes of the partial waves.

The results of the computer simulation and the chain of such OVs experimentally obtained upon interference of two plane waves with approximately equal intensities and with the probe reference beam are illustrated in Fig. 6. The vortex phases in adjacent intensity minima differ by π , that is, the OVs of the same sign are observed.

Additional possibilities in a purposeful creation of controllable arrays of the vortex-type singularities are supplied by the multiple-plane-waves interference [125–128]. The fields generated in this way can be treated as ordered speckle fields, and just like the stochastic

speckle patterns [11, 61], they demonstrate strict association between the bright speckle spots and the adjacent OVs.

3.2. Generation of polarization singularities on the base of two-wave interference

Like the phase singularities appear in points where the phase is indeterminate [20, 35, 38], the polarization singularities are a type of optical singularities that arise when one of the parameters specifying the polarization of the light is undefined [23, 129]. Particularly, C-points are singularities present in a field of polarization ellipses, where the orientation of the ellipse is undefined; s -contours are lines where the polarization handedness is indeterminate (the polarization is linear). The C-point is a point with the perfect circular polarization where the instantaneous transverse electric vector rotates (without changing its module). A C-point is surrounded by a field of ellipses whose major semi-axis rotates about the C-point. This divides the C-points into two classes: those near which the ellipses rotate together with the angular coordinate about the C-point, and those where the ellipses rotate counter to it. An index representing this rotation about the C-point is called Poincare index (I_C) [130]. Since ellipses axes are not directional, the minimum rotation is half a turn, and so the smallest absolute value of I_C is 1/2. In addition to the rotation, the ellipses form a pattern that can be divided into three classes: lemon, star, and monstar [23] (see Fig. 7). Lemon and monstar have $I_C = +1/2$, and star has $I_C = -1/2$.

The lines shown in Fig. 7 are formed by following the directions of the major semi-axis of the polarization ellipses; the red lines highlight the situations where the semi-axis directions are radial. These lines help to understand the value of I_C for each case. For cases (a) and (c), a vector aligned with the lines rotates in a counter-clockwise sense for a counter-clockwise circulation around the C-point. Conversely, in case (b), a vector rotates in the opposite, clockwise sense, for a counter-clockwise circulation. The lemons [Fig. 7(a)] have only one direction where the major semi-axis is radial: the major semi-axis rotates at half the rate of circulation about the C-point, and so there is undoubtedly one direction where the axis points to the centre (C-point). The same is true with the star [Fig. 7(b)]: since here the ellipses rotate in the sense opposite to the path, the axis must be radial in three places. For the monstar [Fig. 7(c)] the pattern is not obvious. This is because the monstar is part of a more general class of C-points where the rate of rotation of the major semi-axis is not constant: the rotation rate may be greater and lower than the circulation rate, creating more than one angular

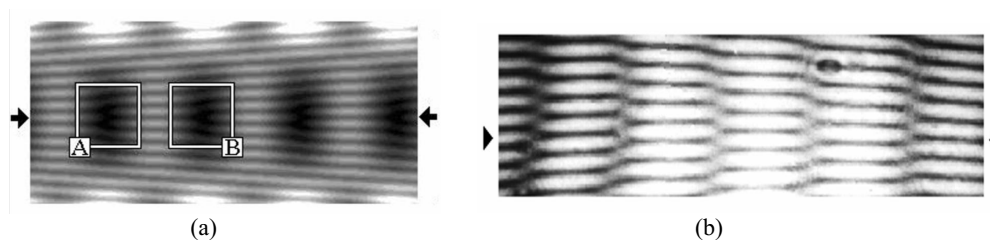


Fig. 6. Demonstration of the emergence of the same-sign OVs in adjacent minima: (a) results of the computer modelling (A, B – OVs), (b) OVs obtained in experiment.

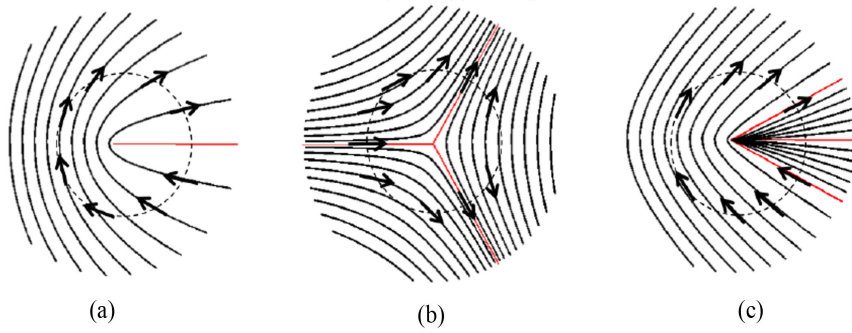


Fig. 7. The three types of C-points: lemon (a), star (b), and monstar (c). The solid lines connect the directions of the major semi-axes of the ellipses. The vectors drawn illustrate how they rotate in a circular (dashed-line) path around the C-point [129].

direction where the polarization ellipses axes are radial. In Fig. 7(c), there are three angles where this is true. These radial directions are separatrices of line morphologies. Also, note something unique about the monstar in Fig. 7(c): in two of the sectors delineated by the separatrices, all the lines have the C-point as an end point.

The presented examples convincingly show the close relations between the polarization singularities and the rotational features of a light field. But these relations are even more direct: as is seen from the definition, a C-point with, e.g., perfect right polarization, is thus an isolated zero of amplitude and, therefore, an OV in the field of the left-polarized component, and vice versa. This close similarity between the phase and polarization singularities can be used for a purposeful creation of the latter ones [131].

In the corresponding methods, the superposition of differently polarized waves is employed. For example, the result of a superposition of two plane waves, in particular with orthogonal linear polarizations, is the resulting field with a homogeneous intensity [132, 133] but inhomogeneous polarization, which was proposed for the generation of polarization singularities.

In this case, the polarization of the field varies in separate points from right-circular to left-circular. However, the C-point does not occur because only one condition necessary for its formation is fulfilled – the phase difference between the orthogonal components is $\pm\pi/2$. The second requirement is that the intensities of the interfering waves are exactly the same. In other words, there should be a “point-like” equality of intensities at a point where the phase difference is $\pm\pi/2$. Obviously, this requirement, as

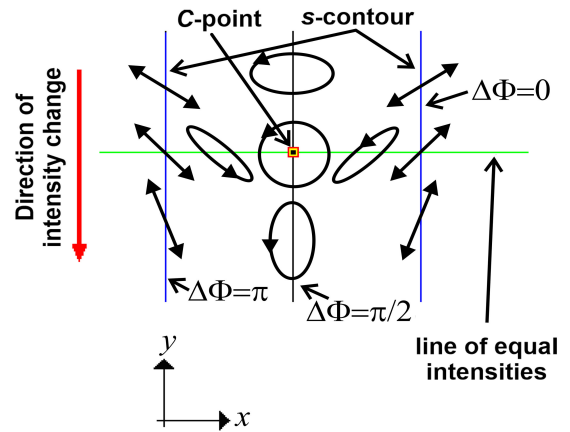


Fig. 8. Polarization modulation of the resulting field between the lines (s-contours) along which the fields u_x and u_y possess the phase difference $\Delta\Phi = 0 + m\pi, m = \pm 1, 2, \dots, n$. The chain of C-points is formed between the lines of equal intensities of the fields u_x and u_y .

in the previous case, can be met if one of the waves has a certain, even small, intensity gradient. Then, in the plane of analysis the distribution of polarization characteristics similar to that shown in Fig. 8 is formed.

The sign of the main phase TC does not depend on the C-point location (no matter if it is on the right or left area) but is determined only by the relations between the amplitude and phase gradients of the waves participating in the superposition. The results of the computer simulation are presented in Fig. 9.

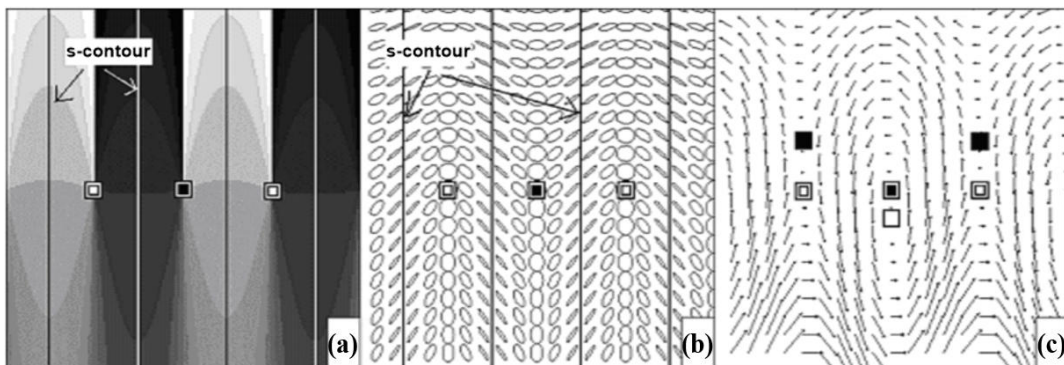


Fig. 9. Three periods of the interference pattern: (a) azimuthal map (distribution of the orientations of the polarization ellipses major axes); (b) view of the polarization ellipses in the resulting field; (c) view of the transverse components of the Poynting vector. Symbols \square , \blacksquare denote positive and negative C-points, \square , \blacksquare – vortex and passive P-singularities, correspondingly.

The sign of the C-point index changes upon transition from one period of the interference pattern to another. Additionally, in Fig. 9, the Poynting singularities are marked, which are shifted with respect to positions of the C-points due to asymmetry emerging in the phase and amplitude distributions of the partial waves [40, 123, 124, 134, 135]. There is a link between the scalar OV's of the separate polarization components and the polarization singularities, associated with the fact that the vortices of the components (arbitrary linear-polarization projection) are situated on the s -contours [39, 122, 123].

For the investigation of such structures, a thin polymer plate was used. The object is selected so that the field scattered by it is “integrally depolarized” with a degree of polarization not higher than 50%. Upon the object illumination by the circularly polarized beam, the s -contours are of small size and contain, as a rule, regions with one handedness of polarization (right or left); such regions do not include nested s -contours. Here, a possibility exists to detect the localization of s -contours as well as the C-points [39, 122, 123, 136]. Herewith, the sum TC of the OV's, corresponding to an arbitrary linearly polarized projection and situated on a single s -contour, is twice higher than the sum index of the C-points enclosed by this contour.

4. Poynting vector singularities

Poynting vector (9) determines the energy flow and momentum distributions in the electromagnetic fields and,

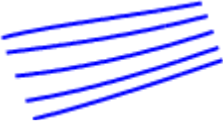




ultimately, the mechanical influence of the light wave on physical objects. Therefore, the vector field of the Poynting vector and its singularities [27, 39, 122, 123, 134, 137, 138] play important roles in all light–matter interactions. In contrast to the spatial distribution of the complete field momentum, which is associated with the 3D Poynting vector distribution, the lines of which are continuous in the light field propagating in the lossless dielectric medium, and the existence of isolated singularities is unlikely [27, 124], the distribution of the transverse Poynting vector can possess the singularities (“P-singularities”) where the vector direction is indeterminate [39, 122, 123].

The full set of singularities allowed by the topological laws includes sources (sinks), hyperbolic point (saddle), centre (vortex), stable and unstable spiral points (foci) (see Table 1).

Like the more traditional phase and polarization singularities, the P-singularities can be combined into networks; each singularity determines (at least at a qualitative level) the Poynting vector behaviour in its vicinity, and the singular network “as a whole” qualitatively determines the transverse Poynting vector at any point of the field: it forms a skeleton for the parameter field of this vector. The characteristics of P-singular skeleton and Poynting vector behaviour in intermediate points of the field are related to the networks of the traditional singularities.

For example, in Fig. 10 the results of the computer simulations are presented for the transverse Poynting vector component in the elliptically polarized Gaussian

Table 1.
Classification of generic singular points in 2D vector fields [27, 32] (following to [139]).

Typical view of the flow lines	Terms and short characteristic
	No singularity (regular point)
	Stable (source) or unstable (sink) node (flow lines go towards or outwards the singular point)
	Hyperbolic point; saddle
	Elliptic point; centre; circulation; vortex
	Stable or unstable spiral point (focus). Flow lines approach to or emanate from the singular point making infinite number of rotations

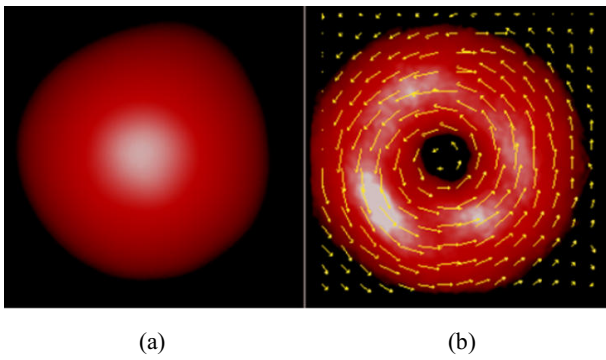


Fig. 10. Calculated results for the transverse Poynting vector circulation in the elliptically polarized Gaussian beam: (a) the intensity distribution, (b) transverse Poynting vector distribution. Colour brightness shows the absolute value, arrows indicate the directions.

beam [138]. In this case, the transverse Poynting vector represents the spin momentum contribution (12), (16) which circulates near the axis and whose “strength” (magnitude) is determined by the radial gradient of the degree of circular polarization ($|u_+|^2 - |u_-|^2$). The characteristic behaviour of the transverse Poynting vector components near some P-singularities, classified in Table 1, is illustrated in Fig. 11.

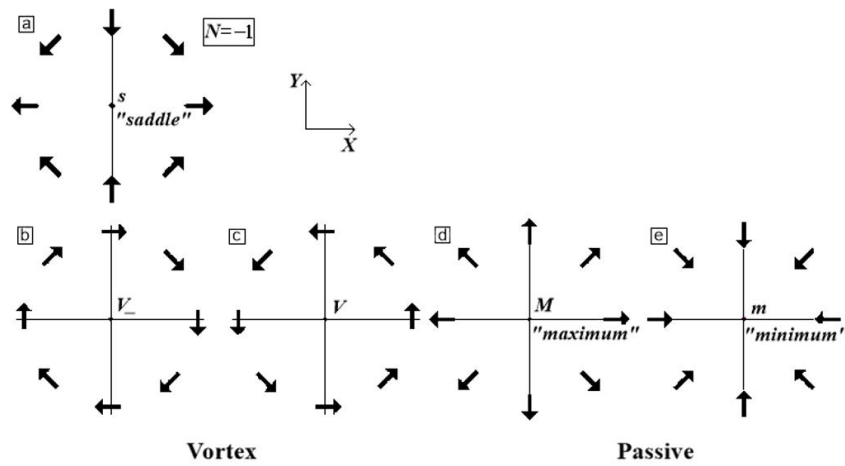


Fig. 11. Behaviour of the transverse Poynting vector near the P-singularities of different five: (a)–(e) types.

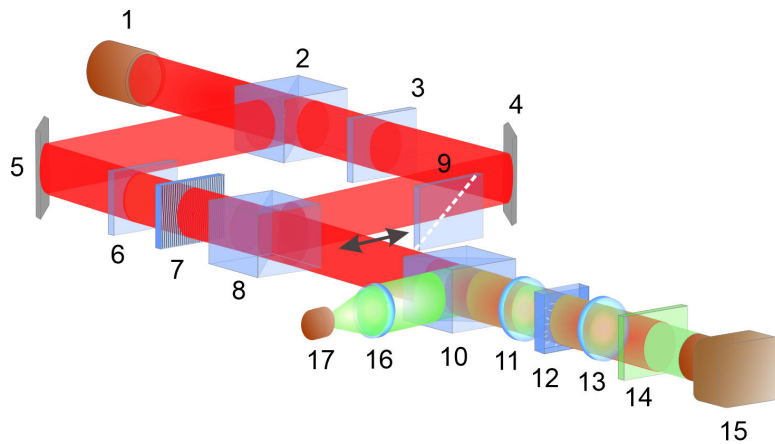


Fig. 12. Experimental scheme for observation of the AM of the polarization trap: 1 – He-Ne laser; 2, 8, 10 – beam-splitters; 3, 6 – $\lambda/4$ plates; 4, 5 – mirrors; 7 – OV-producing computer-synthesized hologram (cf. Fig. 3); 9 – analyser; 11, 14 – micro-objectives; 12 – sample with suspended microparticles; 14 – green filter; 12 – CCD-camera; 16, 17 – system of the sample illumination.

Figure 11 provides additional classification indicators for P-singularities. They can be characterized in terms of the Poincare index (the number of the vector direction rotations on a full trip near the axis). Only for the “saddle” this index is negative. Another classification of the P-singularities is based on the presence of rotation in the singular-point vicinity: for passive singularities (e.g., source or sink), the rotation tends to zero whereas for active (or vortex) singularities (focus, centre) the rotation tends to maximum. As a measure of rotation in these cases, the field AM normalized by the energy included inside the near-axis circle, whose radius tends to zero, can be taken. To distinguish the sense of the near-singularity circulation, the characteristic of “chirality” of the P-point is additionally introduced.

The AM existence in the vicinity of a vortex P-point has been confirmed in experiments performed in the arrangement presented in Fig. 12. A vortex singularity arises when the sign of the topological charge of the main phase in the vicinity of the C-point does not coincide with the sign of the spin factor. It is a consequence of the fact that in the vicinity of such a singularity both orbital and spin angular momenta are of the same direction. A passive singularity appears when both signs of the topological charge of the main phase and of the spin factor coincide.

Since in the upper arm of the interferometer of Fig. 12, a smooth circularly-polarized beam is formed, and in the lower arm, with the help of the “fork” hologram 7, an OV is generated with the opposite circular polarization, in the focal (sample) plane, a focused “full Poincare beam”, first described in [39, 122, 123], is formed with the C-point in the centre. Due to the maximum in the smooth component, such a bright optical trap enabled the stable localization of the particle near the axis, just in the area where the OAM of the oppositely polarized component performs its efficient rotation (Fig. 13). Therefore, the presence of the AM near a C-point singularity is testified.

It should be noted that the positions of the P-singularity and the C-point do not coincide in a general case, and, as is shown in Ref. 134, the P-singularity shift with respect to the C-point position is determined by the degree of phase and amplitude asymmetry of the field. Nevertheless, the connection between the C-points and P-singularities is preserved even in stochastic fields. This is illustrated by Fig. 14 which shows a fragment of a random (speckle) vector field with C-points and P-singularities. To summarize, it can be stated that the definite connection exists between the systems of Poynting-singularities and the polarization singularities. Negative (positive) C-points and the vortex (passive) P-singularities form pairs, and the distance between the P-singularities and associated C-points is determined by the degree of asymmetry of the orthogonal polarization components of the vector field.

5. Vector light fields and the polarization degree of freedom

The light polarization (spin) is an intrinsic degree of freedom which characterizes the intrinsic state of the field, largely independent on its spatial characteristics. At the same time, the deep interrelations exist between the spatial distribution of light and its polarization which can be described and consistently interpreted based on the DCs of the optical field [27, 32, 33, 41, 51, 140], first of all, on the principles of the spin-orbital momentum decomposition (10)–(12). Now, these relations are considered in more detail and, where relevant, without paraxial limitations of (15)–(19); in addition, the distributions of the AM constituents are taken into account.

In the general case of a structured light field, the SAM density is described by equation

$$\mathbf{s} = \frac{g}{2\omega} \text{Im}(\varepsilon \mathbf{E}^* \times \mathbf{E} + \mu \mathbf{H}^* \times \mathbf{H}), \quad (36)$$

i.e., the spin momentum (12) is directly related to $\mathbf{s}(\mathbf{R})$ and originates from its spatial inhomogeneity:

$$\mathbf{p}^S = \frac{1}{2} \nabla \times \mathbf{s}. \quad (37)$$

The OAM density appears directly as the “moment” of the orbital momentum (11),

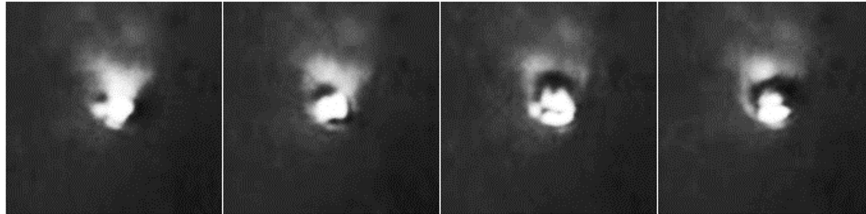


Fig. 13. Rotation of the trapped microparticle due to the AM emerging in the C-point vicinity. The sign of singularity determines the direction of rotation.

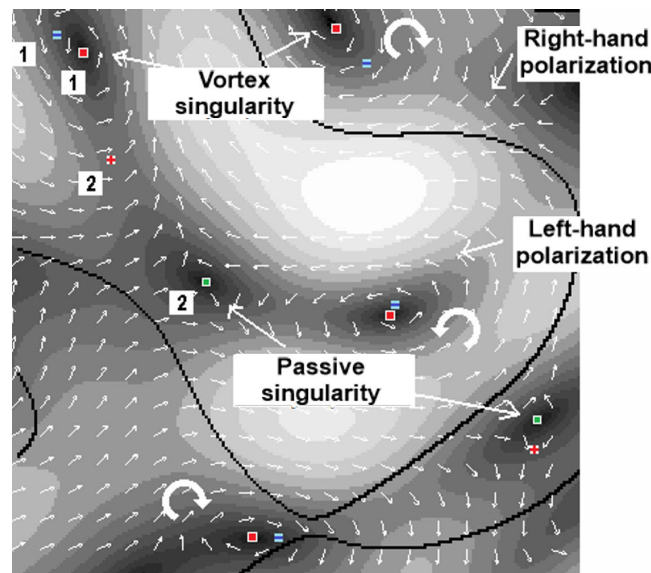


Fig. 14. Correspondence between the C-points and P-singularities: \oplus, \ominus – positive and negative C-points; \oplus, \ominus – vortex and passive P-singularities. Numbers (1) and (2) indicate the pairs of the polarization and P-singularities.

$$\mathbf{L} = \mathbf{R} \times \mathbf{p}^o. \quad (38)$$

This definition differs from the paraxial version (17) because in the general structured fields, there is no well-defined longitudinal axis, and the OAM (38) explicitly depends on the reference point (the frame origin) which can be chosen with a certain freedom. As a result, while the SAM is an “intrinsic” sort of AM which characterizes the energy flows “inside” the beam, the OAM includes the “extrinsic” AM of the beam, as a whole, with respect to a certain “external” centre, as well as the “intrinsic” one measured regarding some physically selected point (or axis) of the beam [141, 142] (e.g., the propagation axis in the paraxial case of section 2.1 [33]).

Although the momentum decomposition into the orbital (“canonical”) and spin (“virtual”) parts encountered in earlier works (in particular, the spin momentum was introduced by Belinfante in the frame of the energy momentum tensor symmetrisation in 1940 [143]), its actualization in the context of structured and singular light fields has proven to be extremely important. It stimulated the further development of the concepts mentioned [27, 32, 33, 144], starting with the Berry’s work [51] (where, by the way, the form of equations (11) and (12) was proposed). Remarkable contributions were made by the authors of this review [25, 140, 145–149].

According to the general concepts [27, 41, 51], \mathbf{p}^o is the source of the OAM, while \mathbf{p}^s is the cause for the SAM which is inherent in circularly and elliptically polarized fields. In previous theories [100, 150, 151], the explanation of the origin of SAM was accompanied by the paradoxical conclusion that in a homogeneous beam the SAM density vanishes; at the same time, any object that absorbs light energy and is located on the beam path experiences its rotational action, and hence, its non-zero SAM.

To solve this paradox, a model was proposed that illustrates the origin of the “spin” energy flux and, accordingly, the spin momentum (12) (Fig. 15) [27, 41, 140]. In a beam with circular polarization, a transverse rotation is associated with the rotation of the instantaneous electric and magnetic vectors. In contrast to the OV-associated circulation presented in Fig. 1, here the energy circulation occurs locally “in each point” which can be imagined as if the circulation of energy occurs inside the microscopic cells. In this pattern, if the beam is homogeneous, the contributions of adjacent cells are mutually compensated, so that the macroscopic flow of energy is absent, and this corresponds to the (seeming) zero

SAM density. The compensation will be incomplete if the adjacent cells are not identical (e.g., differ by the local light intensities), and this explains the non-zero SAM density in a transversely inhomogeneous beam [its relationship with the beam spatial inhomogeneity is directly seen from (37)]. At last, there is no compensation at all when the cell array breaks off, i.e., at the beam boundary. It does not have to be a real physical boundary; no matter how a certain part of the beam cross section is “isolated”, its “boundary” cells become “uncompensated”, and the resultant circulation appears along the boundary of this part which is the origin of the SAM. This circulation is formed by the spin momentum (the transverse orbital momentum is zero in a homogeneous beam), and one can easily show that it equals the sum of contributions from all the enclosed cells. Obviously, it is a sort of “isolation” that takes place when a wave “meets” an object: its projection “cuts out” part of the beam cross section and, thus, leaves some cells without their “compensating” neighbours. The similar explanation of the SAM nature can be developed in the more exquisite mathematical form [152].

As a result, the spin momentum (12) appears as a part of the field linear momentum (or the corresponding energy flow) which originates completely from the rotational properties of light, and it does not exist in fields without such properties (e.g., linearly polarized). The most important features of the optical momentum constituents \mathbf{p}^s , \mathbf{p}^o and their sum \mathbf{p} were studied analytically with a series of examples [27, 32, 41, 153–155], where the typical patterns of the energy flow and momentum distributions in paraxial beams are considered. Particularly, by using the examples of the simplest LG modes (22), it is found that the circulatory spin momentum can be directed oppositely to the orbital momentum, and/or to the circular-polarization handedness of the homogeneously polarized beam. As a result, the total circulatory momentum of the beam with a uniform circular polarization may have different directions in different regions of the cross section which are separated by the contours of zero transverse momentum.

The subsequent research has demonstrated that the orbital momentum is directly related to the processes of energy transfer in the beam; the partial orbital-momentum constituents of the individual polarization components are always directed along the normals to the corresponding wavefronts (cf. Fig. 1). The orbital momentum exists in unpolarized and scalar beams, its direction is determined by the phase gradient, and the transverse orbital momentum is always orthogonal to the equiphase contours. At the same

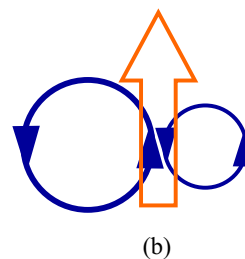
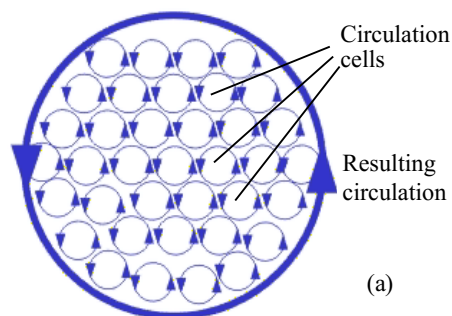


Fig. 15. Illustration of the spin-momentum formation in a circularly-polarized beam: (a) homogeneous beam with a sharp boundary; (b) emergence of the macroscopic energy flow (vertical arrow) in an inhomogeneous beam (different sizes of the circulation loops symbolize different circulation “strengths”).

time, the spin momentum in paraxial beams always lies in the transverse plane [see (13) and (16)] and is proportional to the transverse inhomogeneity of the “third” Stokes parameter, $s_3 = |u_+|^2 - |u_-|^2$, which expresses the presence and “strength” of circular polarization [cf. relations (16) and (18)]. The spin momentum is directed along the lines $s_3(x, y) = \text{const}$, and the total spin momentum of the whole field vanishes:

$$\iiint_V \mathbf{p}^S d^3\mathbf{R} = 0 \quad (39)$$

due to the solenoidal character of the vector field $\mathbf{p}^S(\mathbf{R})$ [see (37)], $\nabla \mathbf{p}^S = 0$.

As any vector fields, the spatial distributions of \mathbf{p}^S and \mathbf{p}^O can possess isolated singular points where the corresponding vector vanishes, has indeterminate direction or module. These singularities form their own networks that are similar to the networks of P-singularities (see section 4, Table 1, Fig. 11) and obey the similar rules. They constitute useful and powerful additional instruments for the meaningful description, characterization, and investigation of structured light fields.

6. Physical manifestations of the optical spin and momentum constituents

One of the most attractive features of the DCs of light fields, as the means for the field description, is the fact that they immediately quantify important physical influences of the field on material objects. In particular, here the mechanical action of light fields on micro- and nanoparticles is considered; in addition to the interest for physical discussion, such phenomena are significant for many modern applications relating to the micro-manipulation techniques [116–118, 156]. Generally, the study of a mechanical action of light on material objects require a detailed analysis of the processes of light scattering and absorption with account for the particle shape and electromagnetic properties [156–163], but the simplified qualitative picture can be obtained when the particle is supposed spherical with the radius a satisfying the Rayleigh scattering criterion $ka \ll 1$ [163–165]. Under these conditions, the light-particle interaction is described by the dipole approximation which enables the full analytical study of the mechanical action of the main ponderomotive factors of the field.

In the dipole approximation, the particle-field interaction is characterized by the electric α_e and magnetic α_m polarizabilities

$$\alpha_e = \frac{\alpha_e^0}{1 - i \frac{2}{3\epsilon} (nk)^3 \alpha_e^0} \approx \alpha_e^0 + i \frac{2}{3\epsilon} (nk)^3 |\alpha_e^0|^2, \quad \alpha_e^0 = \epsilon a^3 \frac{\epsilon_p - \epsilon}{\epsilon_p + 2\epsilon} \quad (40)$$

$$\alpha_m = \frac{\alpha_m^0}{1 - i \frac{2}{3\mu} (nk)^3 \alpha_m^0} \approx \alpha_m^0 + i \frac{2}{3\mu} (nk)^3 |\alpha_m^0|^2, \quad \alpha_m^0 = \mu a^3 \frac{\mu_p - \mu}{\mu_p + 2\mu}, \quad (41)$$

where ϵ, ϵ_p (μ, μ_p) are the permittivity (permeability) of the surrounding medium and of the particle, correspondingly. The mechanical force experienced by such a particle can be presented as [164–168]

$$\mathbf{F} = \mathbf{F}_e + \mathbf{F}_m + \mathbf{F}_{em} \quad (42)$$

where

$$\mathbf{F}_e = \frac{1}{2g\epsilon} \text{Re}(\alpha_e) \nabla w_e + \frac{\omega}{g\epsilon} \text{Im}(\alpha_e) \mathbf{p}_e^O, \quad \mathbf{F}_m = \frac{1}{2g\mu} \text{Re}(\alpha_m) \nabla w_m + \frac{\omega}{g\mu} \text{Im}(\alpha_m) \mathbf{p}_m^O \quad (43)$$

and

$$\mathbf{F}_{em} = -\frac{\omega}{3g} nk^3 \text{Re}(\alpha_e^* \alpha_m) (\mathbf{p}^S + \mathbf{p}^O) + \frac{\omega}{3g} nk^3 \text{Im}(\alpha_e^* \alpha_m) \mathbf{p}^R. \quad (44)$$

In (43), $w_{e,m}$ and $\mathbf{p}_{e,m}^O$ are the “electric” and “magnetic” summands of (8) and (11). These formulas show that the “dual” symmetry between the electric and magnetic fields [51, 169] is destroyed upon interaction with material objects whose electric and magnetic properties are generally different. Particularly, most of the natural media and particles are non-magnetic, $\mu = \mu_p = 1$, and in this case the dipole magnetic polarizability (41) vanishes. However, it appears in the higher orders of the Mie scattering expansions [163–165] due to interference between the electric and magnetic dipole scattering, and can be presented in the form

$$\alpha_m = (nk)^2 a^5 \frac{\epsilon_p - \epsilon}{30\epsilon}. \quad (45)$$

First summands of expressions (43) represent the gradient force originating from the inhomogeneous energy distribution. The second summands, expressing the “scattering force” (“light pressure force”), distinctly demonstrate the physical relevance of the field momentum decomposition (10): indeed, at least for the dipole mechanical action, not the whole momentum but its part (here, the orbital one) is an influential factor. At the same time, (44) shows that, in addition to the separate “magnetic” and “electric” actions described by (43), a “combined” electric-magnetic action exists associated with other ponderomotive factors. In particular, the first summand in (44) describes the possible mechanical action of the spin momentum \mathbf{p}^S (12), (37) (it can be well separated, for example, in points where the orbital momentum \mathbf{p}^O vanishes or is directed differently; also, \mathbf{p}^S inverts the sign with reversing the sense of circular polarization while \mathbf{p}^O in many cases remains the same). Besides, the second line of (44) indicates the new ponderomotive factor – the “reactive momentum” of the field [170, 171]:

$$\mathbf{p}^R = \frac{g}{c} \epsilon \mu \text{Im}(\mathbf{E}^* \times \mathbf{H}). \quad (46)$$

In the dipole approximation, the particle may “feel” not only the translational action described by the force (43) and

(44) but also the rotational one. The latter is characterized by the field-induced torque [165,168]

$$\mathbf{T} = \frac{\omega}{g} \left[\frac{1}{\varepsilon} \text{Im}(\alpha_e) \mathbf{s}_e + \frac{1}{\mu} \text{Im}(\alpha_m) \mathbf{s}_m \right]. \quad (47)$$

Note that according to (47), the rotational action on small particles is “simpler” for interpretation because it depends on the smaller number of different competing factors than the translational force. It looks a bit paradoxical that the torque (47) does not include the OAM, which is the source of rotations in optical spanners discussed in section 2.5. This can be explained by reasoning that in the OAM-based optical spanners [116–118] the torque appears due to a combination of eccentric optical forces generated by the vortex orbital-momentum distribution [172], and the particle size is large enough to feel the different forces exerted at different points of the particle “body”. In relation (47), the particle is supposed to be smaller than any spatial variations of the field, responsible for the OAM, and the only torque “felt” by the particle is from the absorbed

SAM. This circumstance can be used for the experimental investigation of the “pure” SAM and, on the other hand, when the field characteristics are known and well controllable, for the study of the particle properties [160] (see Fig. 16).

According to (40)–(45), for small particles with $ka \ll 1$, the optical force and torque dependence on the particle size a is of the power-law character, and the power exponent can be a characteristic marker of the corresponding ponderomotive factor reflecting the physical nature of its mechanical action [162, 164] (see Fig. 17). The gradient force F_y^{grad} increases as a^3 , the light-pressure force from the orbital momentum F_{orb} is proportional to a^3 for the absorbing and to a^6 for non-absorbing particles. The spin-momentum force F_{sp}^\pm emerges due to the interference between the electric and magnetic dipole scattering [see (44)]. The lowest order in which it takes place can be observed for the particles possessing both electric and magnetic properties and corresponds to $\sim a^6$.

For non-electric or non-magnetic particles, the force from the spin momentum consists of two terms. The first

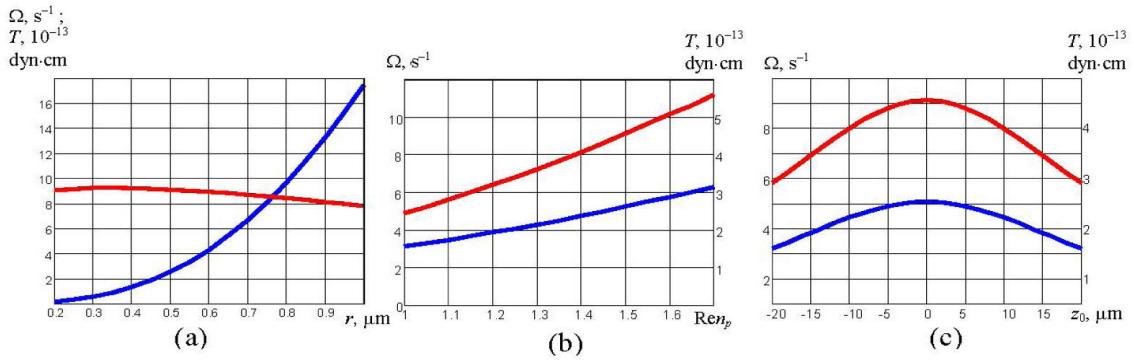


Fig. 16. (Blue) radiation torque and (red) corresponding angular velocity of the spinning motion of the particle with the absorption index $\kappa = 4 \cdot 10^{-4}$ suspended in water and trapped in the centre of the Gaussian beam [160]: (a) $Re n_p = 1.5, z_0 = 0$, particle radius r is variable; (b) $r = 0.5 \mu\text{m}, z_0 = 0, Re n_p$ is variable; (c) $r = 0.5 \mu\text{m}, Re n_p = 1.5, z_0$ is variable. Particle refraction index $n_p = 1.5 + i\kappa$; wavenumber in water $nk = 1.286 \cdot 10^5 \text{ cm}^{-1}$ for wavelength $\lambda = 0.65 \mu\text{m}$. The beam axis coincides with the axis z , and the particle centre is situated at a distance z_0 from the beam waist where its radius is $b_0 \approx 1.4 \mu\text{m}$ and the total power $\sim 100 \text{ mW}$.

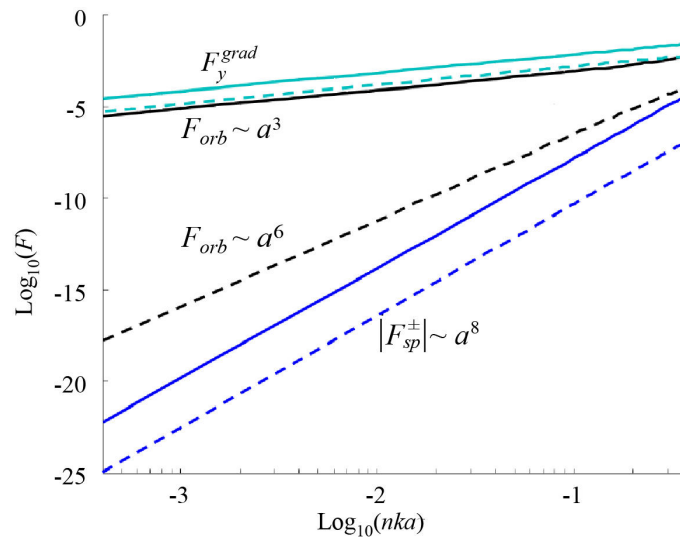


Fig. 17. Calculated force vs. a particle-size parameter presented in a double logarithmic scale. Solid lines: metallic particle (gold particle in water, $n_p/n = 0.32 + 2.65i$), dashed lines: dielectric particle (latex in water, $n_p/n = 1.12$). Orders of the force growth with the particle radius a are indicated with allowance for the normalization factor, obtained by dividing the calculated quantities by the total momentum flow of the incident field through the particle cross section. For comparison, the behaviour of the gradient force F_y^{grad} is included. The radiation wavelength is 633 nm.

term follows from the interaction between the electric and magnetic dipole moments (but due to zero dipole polarizability, one of these moments occurs in higher orders of the expansion in degrees of ka), the second is formed due to the interference between the dipole and quadrupole components of the scattered field. Both contributions depend on the particle size as a^8 . An important conclusion from (41), (44), and (45) is that the spin momentum, unlike the orbital one, can “push” or “pull” a particle regarding its optical properties, electric and magnetic polarizability. Non-magnetic dielectric particles usually move oppositely to \mathbf{p}^S , whereas the conductive particles move along \mathbf{p}^S (the contribution proportional to \mathbf{p}^S in (44) behaves similarly, but the orbital-momentum-induced light pressure of (43) produces, as a rule, the predominant orbital-momentum influence). Of course, translational motions induced by the spin momentum are always accompanied by the spinning of the particle around its own axis stipulated by the torque (47) [153, 160, 164]. Relations (40)–(45) and the condition $ka \ll 1$ make an impression that \mathbf{p}^S produces a much weaker force than the energy gradient or the orbital momentum \mathbf{p}^O . However, this is only correct for the subwavelength particles. The numerical analysis has shown [161, 162, 173] that when $ka \gtrsim 1$, all ponderomotive factors perform comparable mechanical actions (see also Fig. 21).

Further experimental efforts were aimed at the detection and quantification of the mechanical action, associated with the spin momentum, beyond the dipole approximation accepted in (44). Preliminary theoretical developments [161–163] employing the model fields formed by interference of the simplest plane waves and numerical calculations highlighted the existence of the spin-momentum force able to move spherical microparticles, as well as situations where such a force can be geometrically separated from other optical forces (light pressure, gradient force) and reliably detected.

The first experimental observation of the spin-momentum force was obtained by using the spatially inhomogeneous circularly-polarized light [174–176]. In these experiments (Fig. 18), two identical beams obtained from a semiconductor laser ($\lambda = 0.67 \mu\text{m}$) with the radii $b = 0.7 \text{ mm}$ (measured at the intensity level e^{-1} of maximum) approach a micro-objective with focal distance $f = 10 \text{ mm}$. The beams are parallel to the micro-objective axis and are located at a distance $a = 1.3 \text{ mm}$ from it,

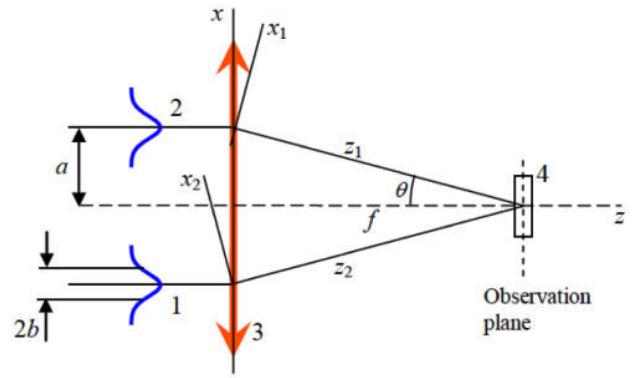


Fig. 18. Schematic of the experimental setup: (1), (2) input beams, (3) objective lens schematized by the double arrow, (4) cell with probing particles suspended in water. Axes x_j and z_j of the involved frames are shown, axes y_j are orthogonal to the figure plane.

which provides the effective focusing angle $\theta = \arctan(a/f) \approx 7.4^\circ$ and $\text{NA} = 0.16$; after focusing, they interfere in the focal region of the micro-objective.

In the focal plane, the 3-lobe interference pattern is formed (Fig. 19). A latex particle ($n_p = 1.48$) is trapped within the central lobe at a certain distance from the axis due to the equilibrium between the gradient force “pulling” it to the intensity maximum and the orbital-momentum-induced light pressure “pushing” it out [cf. the first equation (43)]. If the incident beams 1 and 2 (Fig. 18) are circularly polarized, the asymmetric particle spins due to the spin-induced torque (47). Simultaneously, it performs an orbital motion [dashed elliptic trajectory in Fig. 19(c)] due to the transverse spin-momentum (16) and the corresponding force component [first summand of (44)]. Note that in this scheme, the light pressure does not contribute to the particle motion but merely keeps it inside the region where the spin-momentum is maximal. Note that the particle orbits against the spin momentum [cf. panels (a) and (c)]. Its orbiting reverses the sense with switching the sign of circular polarization; in case of linear polarization, the particle motion stops.

Experimental results relating to detection and evaluation of the mechanical action of the optical spin and spin momentum [149, 160, 174–176] indicate the possibility of their application in the micromanipulation techniques in which the regulation and switching of the regimes is carried out by controlling the polarization,

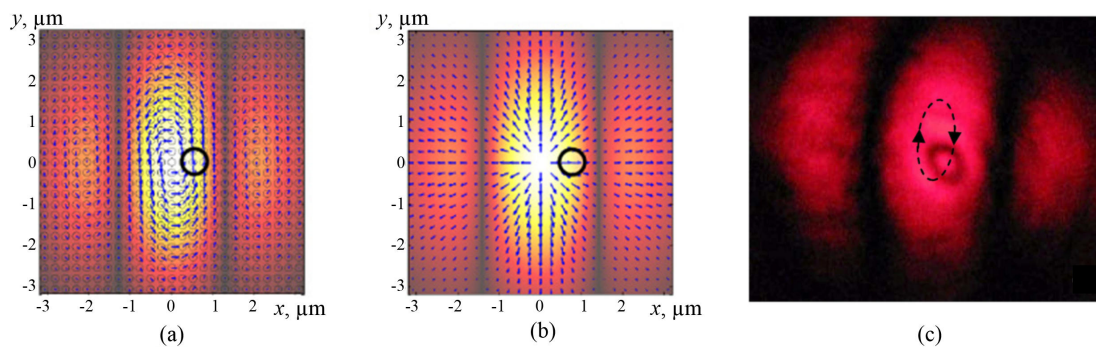


Fig. 19. Characteristics of the optical field in the observation plane for $\sigma = 1$ ($\sigma = \pm 1$ denotes the polarization handedness), viewed against the z -axis: (a) spin-momentum and (b) orbital-momentum maps (arrows) with the intensity distribution as a background; (c) view of the trapped particle and the trace of its motion. In panel (a), polarization ellipses are shown on the background (because of small θ , they have small eccentricities and visually look like circles); panels (a) and (b) also contain contours of a trapped particle (black circle).

without changes in the intensity or spatial profile of the beam. This technique can offer advantages due to the almost complete absence of power loss and the high regulation speed.

From the fundamental point of view, the possibility and peculiar features of the spin-momentum-induced particle motion reveal the special properties of the spin degrees of freedom of the electromagnetic field and the prospects for their experimental study. The rotational action of the SAM can be used for a measurement of the weak absorption of small particles [160] which is difficult to perform in a direct way. In addition to the consistent calculations of the rotational action produced by the optical OAM and SAM, based on the Mi theory, a simplified “ray” model of rotation and forced orientation of particles trapped inside beams of different nature has been developed [172]. Based on the principles of geometrical optics, it is applicable for relatively large particles of arbitrary shape (which often occurs, for example, in aerosol studies). It is assumed in this model that each ray carries a momentum and an angular momentum proportional to the local density of these quantities, and the interaction of the field with the particle is calculated by means of the usual geometric-optics principles. The results can be useful, among other things, for exploiting the optical levitation traps and in the studies of the angular distribution of scattering from complex objects.

7. Extraordinary manifestations of structured light fields

The system of DCs introduced and elaborated in the previous sections [27, 32, 33, 41, 51] has proven its effectiveness in application to special highly-structured and localized optical fields [25, 26, 28]. An example of such

fields is offered by the evanescent waves (EWs), strictly localized near the boundaries between materials with different optical properties (Fig. 20). Their meaningful description essentially involves the concepts of spin-orbital interactions, intrinsic rotations and the spin-orbital momentum decomposition (10) [165, 177–182].

In the EW, the electric and magnetic fields exponentially decay with growing off-interface distance x ; if the medium refractive index is n , they can be described by equations:

$$\mathbf{E}(\mathbf{R}) = \frac{A}{\sqrt{1+|m|^2}} \left(1, m \frac{nk}{k_z}, -i \frac{\kappa}{k_z} \right)^T \times \exp(ik_z z - \kappa x) \quad (48)$$

$$\mathbf{H}(\mathbf{R}) = \frac{A}{\sqrt{1+|m|^2}} \sqrt{\frac{\varepsilon}{\mu}} \left(-m, \frac{nk}{k_z}, im \frac{\kappa}{k_z} \right)^T \times \exp(ik_z z - \kappa x), \quad (49)$$

where $k_z > nk$, $\kappa^2 + k_z^2 = (nk)^2$, and A is the amplitude factor. Formally, (48) and (49) describe a plane wave with the complex wavevector

$$\mathbf{k} = \mathbf{e}_z k_z + \mathbf{e}_x k_x = \mathbf{e}_z k_z + i \mathbf{e}_x \kappa \quad (50)$$

whose real and imaginary parts are orthogonal, $\text{Im } \mathbf{k} \perp \text{Re } \mathbf{k}$ [see Fig. 20(a)]. The parameter m characterizes the polarization state and can be related to the “Stokes parameters”:

$$\tau = \frac{1 - |m|^2}{1 + |m|^2}, \quad \chi = \frac{2 \text{Re } m}{1 + |m|^2}, \quad \sigma = \frac{2 \text{Im } m}{1 + |m|^2}. \quad (51)$$

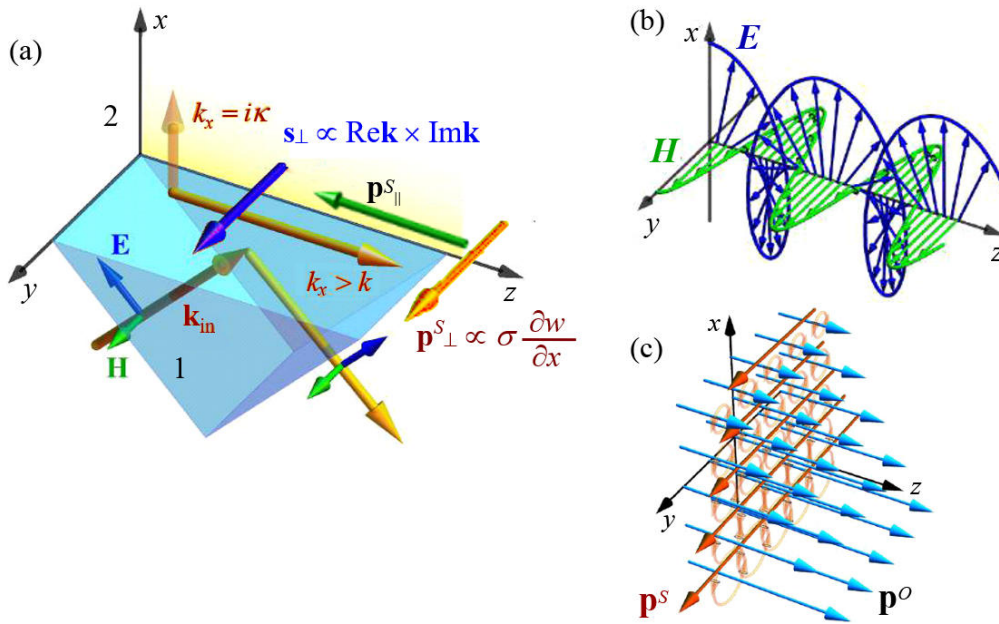


Fig. 20. EW and its characteristics: (a) EW generated by the total internal reflection of a plane wave with the wavevector \mathbf{k}_{in} [arrows show the wavevectors, transverse extraordinary spin (blue), and spin momentum (brown)]; (b) z -distribution of the instantaneous electric and magnetic fields \mathbf{E} and \mathbf{H} for the simplest linear x -polarization [TM mode with $m = 0$, $\tau = 1$, see (51)]; (c) cross section of the EW with non-zero σ (51) [blue arrows show the OM lines \mathbf{p}^o (with exponential decay in the vertical x -direction), closed loops, squeezing with growing x , symbolize the elliptical polarization whose inhomogeneity generates the transverse SM \mathbf{p}^s].

The energy density w , the orbital \mathbf{p}^O and spin \mathbf{p}^S momentum densities, and the SAM density \mathbf{s} of the EW field, presented by (48), (49), and Fig. 20, are expressed by equations:

$$w = g\varepsilon|A|^2 \exp(-2\kappa x), \quad (52)$$

$$\mathbf{p}^O = \mathbf{p}_e^O + \mathbf{p}_m^O = \frac{w}{\omega} k_z \mathbf{e}_z, \quad (53)$$

$$\mathbf{p}^S = \mathbf{p}_e^S + \mathbf{p}_m^S = \frac{w}{\omega} \frac{\kappa}{k_z} (nk\sigma \mathbf{e}_y - \kappa \mathbf{e}_z), \quad (54)$$

$$\mathbf{s} = \mathbf{s}_e + \mathbf{s}_m = \frac{w}{\omega} \left(\frac{\kappa}{k_z} \mathbf{e}_y + \sigma \frac{nk}{k_z} \mathbf{e}_z \right). \quad (55)$$

These results disclose the specific dynamical properties of the EW. Usually, as is known, propagating optical waves carry the longitudinal (collinear to the main wave vector) polarization-independent momentum, as well as the longitudinal spin with the value depending on the degree of circular polarization. [However, small corrections to this rule are evident even in paraxial beams, see (15) and (16)]. On the contrary, for EWs, the “extraordinary” polarization-dependent momentum [first summand of (54)] and the “extraordinary” polarization-independent spin [first summand of (55)], both orthogonal to the propagation direction, are the main DCs which express the most typical features of their behaviour.

The nature of the transverse spin (55) is understood from expressions (48), (49), and Fig. 20(b): the EW field contains the longitudinal component shifted by phase with respect to the transverse one so that the instantaneous field vector rotates in the longitudinal plane. This rotation does not depend on polarization and represents an example of the “photonic wheel” [30, 31] [Indeed, the picture of the electric field rotation in Fig. 20(b) resembles the trajectories described by spokes of a rolling wheel]. As this spin is spatially inhomogeneous, due to the same mechanism as presented in Fig. 15, it generates the spin-momentum parallel to the z -axis [second summand of expression (54)]. However, this spin momentum is directed oppositely to the orbital one (53). As a result, the total absolute longitudinal momentum, $|p_z^O + p_z^S|$, appears to be less than $|p_z^O|$. Additionally, an EW can carry a “normal” elliptic polarization in the transverse plane (x, y) [see Fig. 20(c)] whose inhomogeneity generates the transverse spin momentum described by the first summand of (54).

According to (40)–(46), all the spin and momentum constituents can perform their ponderomotive actions while the gradient force offers possibilities for a desirable particle localization in the vertical x -direction [183]. Particularly, the longitudinal and transverse spin components (55) may cause the particle rotation within the longitudinal and transverse planes [173, 184, 185]. Moreover, the rotation around the “vertical” axis x can be also detected [147, 148, 173] even though the spin $s_x = 0$ in (55). This is possible because the separate electric and magnetic parts of the spin,

$$\begin{aligned} \mathbf{s}_e &= \frac{w}{2\omega} \frac{nk}{k_z} \left(\frac{\chi}{2} \frac{\kappa}{k_z} \mathbf{e}_x + \frac{\kappa}{nk} (1 + \tau) \mathbf{e}_y + \frac{\sigma}{2} \mathbf{e}_z \right), \\ \mathbf{s}_m &= \frac{w}{2\omega} \frac{nk}{k_z} \left(-\frac{\chi}{2} \frac{\kappa}{k_z} \mathbf{e}_x + \frac{\kappa}{nk} (1 - \tau) \mathbf{e}_y + \frac{\sigma}{2} \mathbf{e}_z \right) \end{aligned} \quad (56)$$

do contain the vertical contributions. In the resulting spin (55), these cancel each other out, but material particles with asymmetric electric and magnetic properties react to \mathbf{s}_e and \mathbf{s}_m differently, and usually the “sensitivity” to \mathbf{s}_e is much higher.

The orbital momentum (53) performs the usual light-pressure action in the direction of the wave propagation. However, since $k_z > nk$, the ponderomotive action in the longitudinal direction appears to be higher than, for example, in a plane wave with the same intensity [165] [the longitudinal spin momentum of (54) performs a comparatively small mechanical action]. On the contrary, the transverse spin momentum p_y^S is much more “visible” because it performs the polarization-dependent mechanical action in the transverse y -direction [165, 173]. Additional transverse force following from (44) occurs due to the reactive momentum (46) which in the EW of (48)–(51) equals

$$\mathbf{p}^R = \frac{w}{\omega} \frac{nk\kappa}{k_z} \left(-\tau \frac{nk}{k_z} \mathbf{e}_x - \chi \mathbf{e}_y \right). \quad (57)$$

The expected mechanical action of its y -component is similar to that of the spin momentum but depends on the Stokes parameter χ signifying the role of the $\pm 45^\circ$ polarization rather than on the circular-polarization index σ (51).

The qualitative conclusions made on the basis of the DC expressions (53)–(57) and the dipole approximation (40)–(47) are supported by the numerical calculations for particles with moderate sizes $ka \gtrsim 1$ that were performed based on the Mie theory [163, 165]. The numerical analysis of the EW scattering and the corresponding mechanical actions is greatly facilitated by the circumstance that the EW can formally be considered as a plane wave inclined by an imaginary angle [159]. Some results obtained with this approach are illustrated in Fig. 21, and they convincingly testify that the “extraordinary” spin and momentum of the EW can cause quite detectable translational and spinning motions of a particle.

In addition to the known radiation-pressure longitudinal force, vertical gradient force and longitudinal helicity-dependent torque, extraordinary forces and torques appear. The σ -independent torque T_y indicates the transverse helicity-independent spin in the EW. The vertical χ -dependent torque T_y reveals the presence of the vertical electric spin (56) in the diagonally polarized evanescent waves. Finally, the σ - and χ -dependent transverse forces F_y unveil the presence of the transverse spin momentum (54) and the reactive momentum (46), (57).

Note that the transverse components of the spin and momentum exist despite the seemingly planar nature of the system (all “events” occur in a plane parallel to the boundary $x = 0$), and, therefore, are called “extraordinary”. The transverse components arise because the external symmetry associated with the plane interface characterizes only the external degrees of freedom of the wave field, while the polarization degrees of freedom and their associated properties remain, in fact, three-dimensional.

Importantly, the direction of the extraordinary SAM is strictly related to the direction of the EW propagation (“spin-momentum locking”) which opens the possibility for the selective unidirectional excitation of surface optical

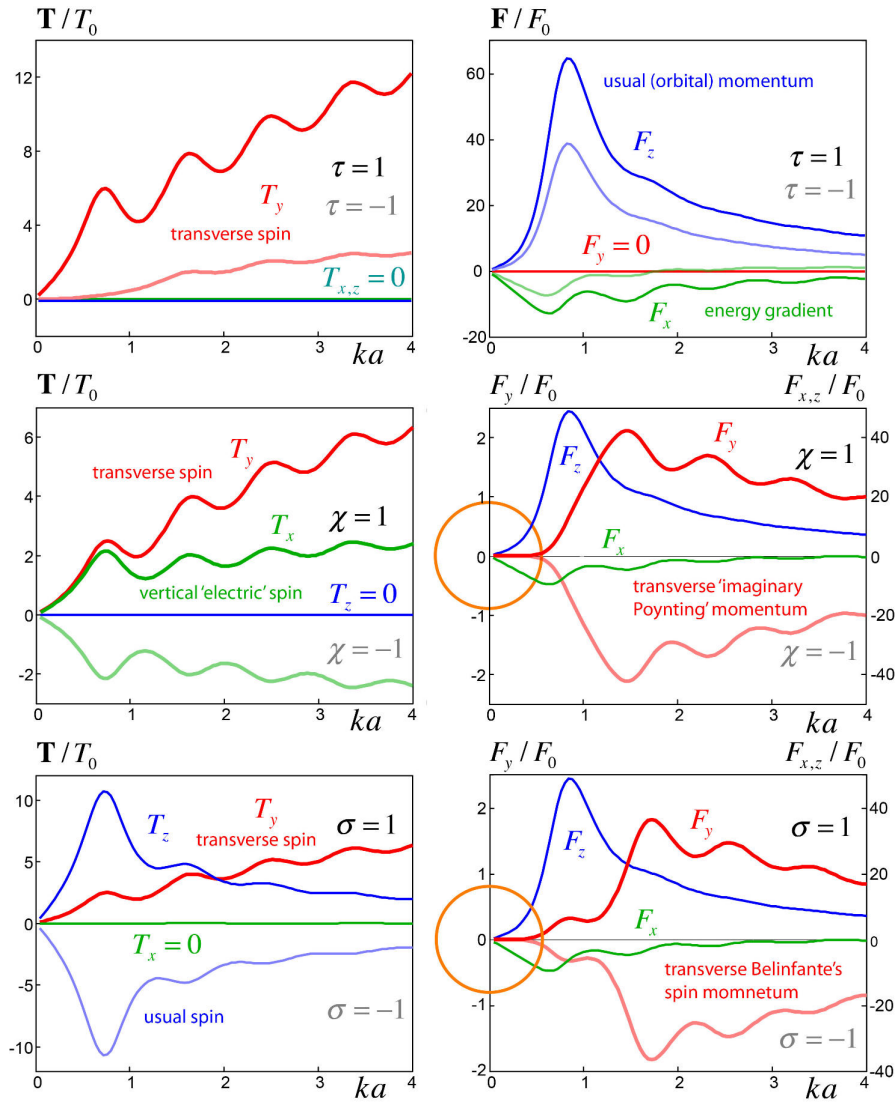


Fig. 21. Radiation forces ($F_{x,y,z}$) and torques ($T_{x,y,z}$) vs. the particle size ka , calculated for a gold Mie particle ($n_p/n = 0.32 + 2.65i$) in the EW field. All components of the forces and torques are shown for six basic polarizations [see (51)]; linear $\tau = \pm 1$, diagonal $\chi = \pm 1$, and circular $\sigma = \pm 1$; orange circles indicate the regions where the dipole approximation (40)–(45) is valid, and the extraordinary transverse forces are negligible (cf. Fig. 17).

waves by choosing the circular polarization of the exciting radiation [181, 182].

Discovery of the extraordinary DCs in the EWs stimulated a great number of works dedicated to the search of new versions of transverse spin and momentum in various wave systems (see, for example, Refs. 27, 31, and 33). Particularly, the rich and non-trivial structure of the spin and momentum distributions is characteristic for the simplest field formed by the interference of two monochromatic waves with non-collinear wave vectors [161, 177]. Like an EW, such a field is seemingly planar in nature, but it shows a transverse (orthogonal to the plane of both wave vectors) helicity-independent SAM and the polarization-dependent spin momentum. The results of modelling the interaction of such fields with the test microparticles show the possibility of direct detection of extraordinary DCs.

Much effort has been undertaken to detect and measure the extraordinary spin and momentum associated with EWs. Measurements of the transverse force with an accuracy of 10^{-15} N were performed with application of the

nano-cantilever placed in the EW formed near the glass surface in the total-reflection regime [178]. These results clearly prove the presence of optical forces orthogonal to the wave vector and proportional to the degree of circular polarization. Simultaneously, the existence of the transverse polarization-dependent force component, caused by the reactive momentum (57), has also been proven.

A series of works [186–191] deal with observations of the EW-induced motions of micro-objects in the water suspension (Fig. 22). In experiments [148, 186, 187], the plate of polyethylene terephthalate (PETP) with dimensions of $200 \times 200 \times 9 \mu\text{m}^3$ floats over the water layer, and the incident beam parameters are adjusted so that the incident wave experiences the total reflection at the upper surface of the PETP plate and approaches it being linearly polarized at 45° . The incident beam is formed by the IR laser radiation ($\lambda = 980$ nm) focused onto a focal spot of $\sim 50 \times 50 \mu\text{m}^2$. As a result, an evanescent wave is formed in the air above the plate, and the total-reflected wave obtains an elliptic polarization, i.e., non-zero vertical spin.

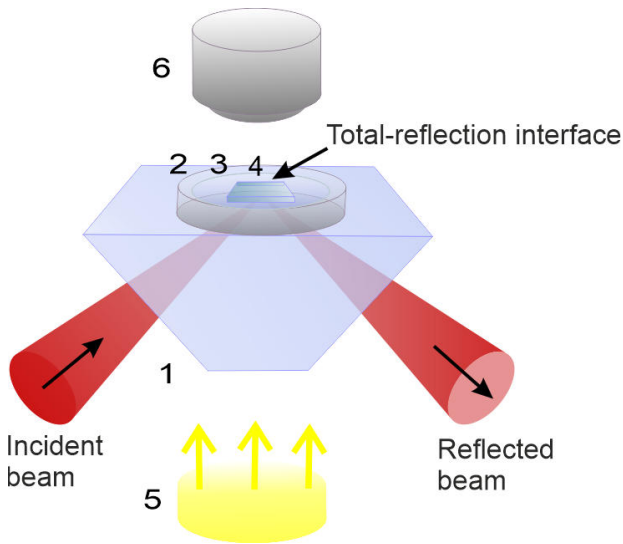


Fig. 22. Experimental arrangement for the detection of the EW-induced motion: (1) glass-cut rectangular prism (refraction index equals 1.52); (2) 2-mm-high ring cuvette; (3) water layer; (4) crystalline plate; (5) white-light illuminating source; (6) CCD camera [148, 186, 187].

Accordingly, the spin density s_x is generated inside the plate, which causes its rotation (see Fig. 23). Simultaneously, the plate performs a translational motion caused by the orbital-momentum force. In fact, these experiments measure the vertical AM transmitted from the incident beam in the reflection process, i.e., reproduce the idea of Beth's first detection of the AM light [8], but indirectly demonstrate the vertical spin s_{ex} of the EW [see first term of the first equation (56)].

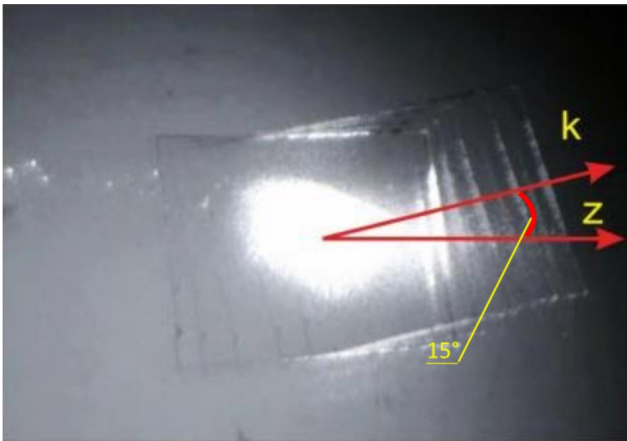


Fig. 23. Motion of a birefringent microplate in the transverse direction under the action of EW [186].

Further experiments [188–191] used the arrangement similar to that of Fig. 22 but the incident beam was adjusted so that the total reflection occurred at the prism 1 surface, and the water layer 3 in the cuvette 2 was completely inside the EW field. This configuration permitted to observe the EW-induced motions of the erythrocytes and other blood cells floating in water. Figure 24 clearly shows both the transverse and (much weaker) longitudinal displacements of the cell. The extent and direction of the transverse displacement could be reversed upon changing the incident beam polarization.

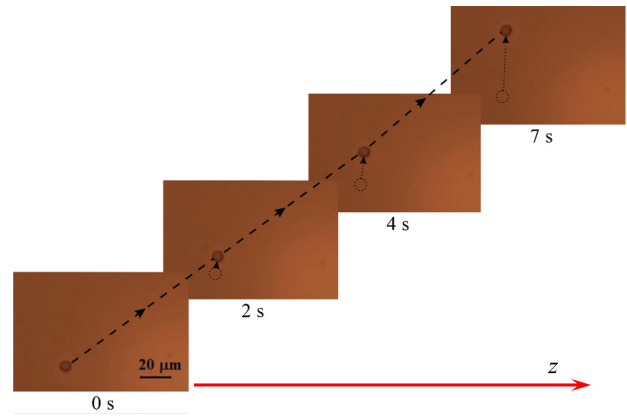


Fig. 24. Motion of an erythrocyte in time.

8. Conclusions

To conclude the current presentation, the authors would like to summarize the main research issues, associated with the studies of optical singularities and related rotational phenomena, that were displayed in the above sections. This review presents an attempt of a general and systemic description of the structured light fields based on the deep intimate associations between the singularities and the rotational phenomena in light; and, indeed, diverse manifestations of this paradigm can be found in many features of the light-field structures or physical actions. The rotational features of the light field are naturally coupled with its specific dynamical characteristics (spatial distributions of energy, momentum, angular momentum, as well as their derivatives) and with dynamical aspects of the light–matter interaction. These, in turn, provide fruitful ideas and powerful instruments for the structured-light analysis and characterization.

This deep, general, and physically meaningful approach appears to be relevant and productive when applied to many physically consistent and practically important special cases. First, an OV has been described as a generic prototype of optical singularities, and OV-related dynamical characteristics (energy flow, momentum and spin distributions) have been scrutinised in detail. The difference exists between the “small-scale” vortex behaviour typical for complex beams with singular networks, and the “global” rotational properties of circular OV beams of the standard families (e.g., the LG_p^l modes). For the latter, the concept treating the OV beam as a rotating mechanical body is described which enables the consistent and meaningful introduction of its mass, moment of inertia, angular velocity, and kinetic energy of rotation. The transformations of such beams in deformable optical systems are associated with the mechanical interactions between the beam field and the optical elements. On this basis, the mechanical interpretation of the rotational Doppler effect has been formulated which discloses additional features of its physical nature and mechanisms. The discussion of the non-collinear rotational Doppler effect links the observed phenomena to the topological-phase manifestations.

The main features of the interference between the OVs and the “usual” smooth-wavefront light beams have been described, and it is shown how the specially

synthesized interference patterns are used for the generation of OV with desirable properties.

It is demonstrated that the rotational features of the “visible” time-averaged optical field are directly connected with the “running” picture of the instantaneous field oscillations that occur with the optical frequency. Remarkably, the orbital momentum (orbital angular momentum) of the average field appears as a natural kinematic characteristic of the translational (rotational) behaviour of the instantaneous oscillations.

The rotational properties of light are naturally classified and interpreted with an explicit involvement of differences and interrelations between the spatial (“orbital”) and polarization (“spin”) degrees of freedom. The meaningful description of the corresponding phenomena is based on the principles of spin-orbital (“canonical”) decomposition of the “full” field momentum (or the energy flow) into the spin and orbital parts. The mathematical features and physical peculiarities of the orbital and spin momenta, specific aspects of their relations to the polarization and spatial properties of light, their physical and mechanical manifestations and possibilities for their detection and measurement have been the subjects of the careful analysis.

Particularly, the polarization singularities were considered in close relations with the patterns of energy flows and momentum distribution in light fields. The polarization singularities were shown to be interrelated with the singularities of transverse energy flow (P-singularities); all systems of singularities form coherent networks qualitatively characterizing the field “as a whole”.

The dynamical characteristics of practically important and physically representative structured fields, especially of evanescent waves and of the two-wave superpositions, have been theoretically investigated. Existence of the extraordinary (orthogonal to the wave vector) polarization-dependent momentum and polarization-independent spin has been shown and explained. Principles of the mechanical action of such fields are studied analytically for the Rayleigh particles (in the dipole approximation) and numerically in the frame of the Mie scattering model. The experimental confirmations of the theoretical predictions were described.

At the same time, the authors must emphasize that the world of optical singularities and associated rotational phenomena is very wide and this review inevitably offers its truncated and blurred image. Many important topics were only mentioned. For example, the vivid activity dealing with the specific interactions between the singular light fields and material media, including the waveguides, optical fibres [47], media with the chiral properties [192, 193], as well as non-linear singular optics [19, 194, 195], is left beyond the present scope. Another significant branch of research concerns the fine details of OV generation methods considered in section 3.1. The knowledge of specific features of the OV beams obtained with the help of different vortex-generating elements, sensitivity of the generated field structures to misalignments, regularities of the transformations performed in case when the incident beam is already singular – all these problems are important not only ‘per se’ but for new fruitful approaches to the optical diagnostics and metrology [54].

Finally, there is a very interesting and meaningful group of phenomena in which the “intrinsic” rotational properties of light (normally “hidden” in circular-vortex beams or non-singular beams with circular polarization) “come to light” due to breaking the beam symmetry [142]. An important special case is represented by the edge or slit diffraction of OV beams [196–200]: here, even a small violation of the circular symmetry leads to a singularity shift from the initial axial position, and, with further propagation, the singularity (or multiple singularities, if the incident OV was multicharged) describe the spiral-like 3D trajectories, brightly illustrating the helical nature of the OV beams [196].

Another case of the symmetry breakdown is realized when the circular beam changes its direction due to refraction or reflection at a plane interface [201–204]. In beams with circular polarization, the spin-orbit interaction [182] contributes to formation of an OV in the longitudinal component of the beam field [second summands in brackets of (3) and (4)]. This leads to specific asymmetric transformations of the beam (optical Hall effect) [200, 204, 205–207] expressed, for example, by the famous Goos-Hanchen and Imbert-Fedorov shifts [207]. These effects supply very impressive manifestations of the influence performed by the intrinsic energy flows on the “extrinsic” behaviour of the beam “as a whole” and testify to the crucial role of the longitudinal field component in the optical Hall-transformations of polarized beams.

All this convincingly indicates that the rotational properties and singularities of light offer a huge area of fruitful research, equally valuable for the fundamental and applied purposes, and promising new fascinating phenomena together with practically useful results.

References

- [1] Descartes, R. *Principia Philosophiae*. (Amsterdam, 1644); *Dioptrique, Meteores*. (Leyden, 1637).
- [2] Descartes, R. [*The World*]. *Le Monde, Ou Traité De La Lumière*. (Abaris Books, 1979).
- [3] Fresnel, A. *Œuvres Complètes*. (Imprimerie Imperiale, France, 1866–1870). (In French)
- [4] Faraday, M. *Experimental Researches in Chemistry and Physics*. (Taylor & Francis, 1859). <https://doi.org/10.5962/bhl.title.30054>
- [5] Maxwell, J. C. *Treatise on Electricity and Magnetism*. (Cambridge University Press, 1873). <https://doi.org/10.1017/CBO9780511709333>
- [6] Sadowsky, A. *Acta et Commentationes Imp. Universitatis Jurievensis (olim Dorpatensis)* 7, 1–3 (1899). (In Russian)
- [7] Poynting, J. H. The wave motion of a revolving shaft, and a suggestion as to the angular momentum in a beam of circularly polarised light. *Proc. R. Soc. Lond. A* **82**, 560–567 (1909). <https://doi.org/10.1098/rspa.1909.0060>
- [8] Beth, R. A. Mechanical detection and measurement of the angular momentum of light. *Phys. Rev.* **50**, 115–125 (1939). <https://doi.org/10.1103/PhysRev.50.115>
- [9] Ignatowski, W. S. Diffraction by a lens of arbitrary aperture. *Trans. Opt. Inst.* **1**, 1–36 (1919). <https://doi.org/10.1017/9781108552264.019>
- [10] Boivin, A., Dow, J. & Wolf, E. Energy flow in the neighbourhood of the focus of a coherent beam. *J. Opt. Soc. Am.* **57**, 1171–1176 (1967). <https://doi.org/10.1364/JOSA.57.001171>
- [11] Baranova, N. B. et al. Wave-front dislocations: topological limitations for adaptive systems with phase conjugation. *J. Opt. Soc. Am.* **73**, 525–528 (1983). <https://doi.org/10.1364/JOSA.73.000525>
- [12] Angelsky, O. V., Maksimyak, P. P., Magun, I. I. & Perun, T. O. On spatial stochastiation of optical fields and feasibilities of optical

- diagnostics of objects with large phase inhomogeneities. *Opt. Spectr.* **71**, 123–128 (1991).
- [13] Couillet, P., Gil, L. & Rocca, F. Optical vortices. *Opt. Commun.* **73**, 403–408 (1989). [https://doi.org/10.1016/0030-4018\(89\)90180-6](https://doi.org/10.1016/0030-4018(89)90180-6)
- [14] Gottfried, K. *Quantum Mechanics*. (Benjamin, 1966).
- [15] Simmonds, J. W. & Guttman, M. J. *States, Waves and Photons*. (Addison-Wesley, 1970).
- [16] Berestetskii, V. B., Lifshits, E. M. & Pitaevskii, L. P. *Quantum Electrodynamics*. (Butterworth-Heinemann, 1982). <https://doi.org/10.1016/C2009-0-24486-2>
- [17] Allen, L., Beijersbergen, M. V., Spreeuw, R. J. C. & Woerdman, J. P. Orbital angular momentum of light and the transformation of Laguerre-Gaussian laser modes. *Phys. Rev. A* **45**, 8185–8189 (1992). <https://doi.org/10.1103/PhysRevA.45.8185>
- [18] Bazhenov, V. Yu., Vasnetsov, M. V. & Soskin M. S. Laser beams with screw dislocations in their wavefronts. *JETP Lett.* **52**, 429–431 (1990).
- [19] Soskin, M. S. & Vasnetsov, M. V. Nonlinear singular optics. *Pure Appl. Opt.* **7**, 301–311 (1998). <https://doi.org/10.1088/0963-9659/7/2/019>
- [20] Soskin, M. S. & Vasnetsov, M. V. Chapter 4—Singular optics. *Prog. Opt.* **42**, 219–276 (2001). [https://doi.org/10.1016/S0079-6638\(01\)80018-4](https://doi.org/10.1016/S0079-6638(01)80018-4)
- [21] Nye, J. F. & Berry, M. V. Dislocations in wave trains. *Proc. R. Soc. Lond.* **336**, 165–190 (1974). <https://doi.org/10.1098/rspa.1974.0012>
- [22] Berry, M. V. Singularities in Waves and Rays. in *Physics of Defects*. (eds. Balian, R., Klaeman, M. & Poirier, J. P.) 453–549 (North Holland Publishing Company, 1981).
- [23] Nye, J. F. *Natural Focusing and Fine Structure of Light. Caustics and Wave Dislocations*. (Institute of Physics Publishing: Bristol and Philadelphia, 1999).
- [24] Gbur, G., Tyson, R. K., Vortex beam propagation through atmospheric turbulence and topological charge conservation. *J. Opt. Soc. Am. A: Opt. Image Sci. Vis.* **25**, 225–230 (2008). <https://doi.org/10.1364/JOSAA.25.000225>
- [25] Angelsky, O. V. et al. Structured light: ideas and concepts. *Front. Phys.* **8**, 114 (2020). <https://doi.org/10.3389/fphy.2020.00114>
- [26] Andrews, D. L. *Structured Light and Its Applications: An Introduction to Phase-Structured Beams and Nanoscale Optical Forces*. (Academic Press, 2011). <https://doi.org/10.1016/B978-0-12-374027-4.X0001-1>
- [27] Bekshaev, A., Bliokh, K. & Soskin, M. Internal fields and energy circulation in light beams. *J. Opt.* **13**, 053001 (2011). <https://doi.org/10.1088/2040-8978/13/5/053001>
- [28] Rubinsztein-Dunlop, H. et al. Roadmap on structured light. *J. Opt.* **19**, 013001 (2017). <https://doi.org/10.1088/2040-8978/19/1/013001>
- [29] Rotenberg, N. & Kuiper, L. Mapping nanoscale light fields. *Nat. Photonics* **8**, 919–926 (2014). <https://doi.org/10.1038/nphoton.2014.285>
- [30] Aiello, A. & Banzer, P. The ubiquitous photonic wheel. *J. Opt.* **18**, 085605 (2016). <http://dx.doi.org/10.1088/2040-8978/18/8/085605>
- [31] Aiello, A. et al. From transverse angular momentum to photonic wheels. *Nat. Photonics* **9**, 789–795 (2015). <https://doi.org/10.1038/nphoton.2015.203>
- [32] Bekshaev, A. Y. & Soskin, M. S. Transverse energy flows in vectorial fields of paraxial beams with singularities. *Opt. Commun.*, **271**, 332–348 (2007). <https://doi.org/10.1016/j.optcom.2006.10.057>
- [33] Bliokh, K. Y. & Nori, F. Transverse and longitudinal angular momenta of light. *Phys. Rep.* **592**, 1–38 (2015). <https://doi.org/10.1016/j.physrep.2015.06.003>
- [34] Dennis, M. R., O’Holleran, K. & Padgett, M. J. Chapter 5 Singular optics: optical vortices and polarization singularities. *Prog. opt.* **53**, 293–363 (2009). [https://doi.org/10.1016/S0079-6638\(08\)00205-9](https://doi.org/10.1016/S0079-6638(08)00205-9)
- [35] Basisty, I. V., Soskin, M. S. & Vasnetsov, M. V. Optical wavefront dislocations and their properties. *Opt. Comm.* **119**, 604–612 (1995). [https://doi.org/10.1016/0030-4018\(95\)00267-C](https://doi.org/10.1016/0030-4018(95)00267-C)
- [36] Soskin, M. S., Vasnetsov, M. V. & Basisty, I. V. Optical wavefront dislocations. *Proc. SPIE* **2647**, 57–62 (1995). <https://doi.org/10.1117/12.226741>
- [37] White, A. G. et al. Interferometric measurements of phase singularities in the output of a visible laser. *J. Mod. Opt.* **38**, 2531–2541 (1991). <https://doi.org/10.1080/09500349114552651>
- [38] Heckenberg, N. R., McDuff, R., Smith, C. P. & White, A. G. Generation of optical singularities by computer-generated holograms. *Opt. Lett.* **17**, 221–223 (1992). <https://doi.org/10.1364/OL.17.000221>
- [39] Angelsky, O. *Optical Correlation Techniques and Applications*. (Bellingham: SPIE Press PM168, 2007). <https://doi.org/10.1117/3.714999>
- [40] Allen, L., Padgett, M. J. & Babiker, M. IV The orbital angular momentum of light. *Prog. Opt.* **39**, 291–372 (1999). [https://doi.org/10.1016/S0079-6638\(08\)70391-3](https://doi.org/10.1016/S0079-6638(08)70391-3)
- [41] Bekshaev, A., Soskin, M. & Vasnetsov M. *Paraxial Light Beams with Angular Momentum*. (New York: Nova Science Publishers, 2008). <https://arxiv.org/abs/0801.2309>
- [42] Gbur, G. J. *Singular Optics*. (CRC Press, 2016). <https://doi.org/10.1201/9781315374260>
- [43] Senthikumar, P. *Singularities in Physics and Engineering*. (IOP Publishing, 2018). <https://doi.org/10.1088/978-0-7503-1698-9>
- [44] Yao, A. M. & Padgett, M. J. Orbital angular momentum: origins, behavior and applications. *Adv. Opt. Photonics* **3**, 161–204 (2011). <https://doi.org/10.1364/AOP.3.000161>
- [45] Barnett, S. M., Babiker, M. & Padgett, M. J. Optical orbital angular momentum. *Philos. Trans. R. Soc. A* **375**, 0444 (2017). <http://doi.org/10.1098/rsta.2015.0444>
- [46] Habraken, S. J. M. *Light with A Twist: Ray Aspects* (Leiden University, Netherlands, 2010).
- [47] Alexeyev, C. N. Propagation of optical vortices in periodically perturbed weakly guiding optical fibres. (Institute of Physical Optics of the Ministry of Education and Science of Ukraine, Lviv, 2010). (in Russian)
- [48] Ruchi, Senthikumar P. & Pal, S. K. Phase singularities to polarization singularities. *Int. J. Opt.* **2020**, 2812803 (2020). <https://doi.org/10.1155/2020/2812803>
- [49] Born, M. & Wolf, E. *Principles of Optics*. (Pergamon, 1968).
- [50] Landau, L. D. & Lifshitz, E. M. *The classical theory of fields. Course of theoretical physics Vol. 2*. (Pergamon, 1975). <https://doi.org/10.1016/C2009-0-14608-1>
- [51] Berry, M. V. Optical currents. *J. Opt. A: Pure Appl. Opt.* **11**, 11094001 (2009). <https://doi.org/10.1088/1464-4258/11/9/094001>
- [52] Haus, H. A. *Waves and Fields in Optoelectronics* (Prentice-Hall, Inc., 1984).
- [53] Bekshaev, A. Y. & Karamoch, A. I. Spatial characteristics of vortex light beams produced by diffraction gratings with embedded phase singularity. *Opt. Commun.* **281**, 1366–1374 (2008). <https://doi.org/10.1016/j.optcom.2007.11.032>
- [54] Bekshaev, A. Y., Karamoch, A. I., Khoroshun, G. M., Masajada, J. & Ryazantsev, O. I. Special features of a functional beam splitter: diffraction grating with groove bifurcation. in *Advances in Engineering Research vol. 28*. (ed. Petrova, V. M.) 1–86 (Nova Science Publishers New York, 2019).
- [55] McGloin, D. & Dholakia, K. Bessel beams: diffraction in a new light. *Contemp. Phys.* **46**, 15–28 (2005). <https://doi.org/10.1080/0010751042000275259>
- [56] Karimi, E., Zito, G., Piccirillo, B., Marrucci, L. & Santamato, E. Hypergeometric-Gaussian modes. *Opt. Lett.* **32**, 3053–3055 (2007). <https://doi.org/10.1364/OL.32.003053>
- [57] Abramovitz, M. & Stegun, I. *Handbook of Mathematical Functions* (National Bureau of Standards, 1964)
- [58] Berry, M. Paraxial beams of spinning light. *Proc. SPIE* **3487**, 6–11 (1998). <https://doi.org/10.1117/12.317704>
- [59] Roux, F. S. Distribution of angular momentum and vortex morphology in optical beams. *Opt. Commun.* **242**, 45–55 (2004). <https://doi.org/10.1016/j.optcom.2004.08.006>
- [60] Bekshaev, A., Orlinska, O. & Vasnetsov, M. Optical vortex generation with a “fork” hologram under conditions of high-angle diffraction. *Opt. Commun.* **283**, 2006–2016 (2010). <https://doi.org/10.1016/j.optcom.2010.01.012>
- [61] Baranova, N. B., Zel’dovich, B. Ya., Mamaev, A. V., Philipetskii, N. F. & Shkunov, V. V. Dislocations of the wavefront of a speckle-inhomogeneous field (theory and experiment). *JETP Lett.* **33**, 195–199 (1981).
- [62] Beijersbergen, M. W., Allen, L., Van der Veen, H. E. L. O. & Woerdman, J. P. Astigmatic laser mode converters and transfer of orbital angular momentum. *Opt. Commun.* **96**, 123–132 (1993). [https://doi.org/10.1016/0030-4018\(93\)90535-D](https://doi.org/10.1016/0030-4018(93)90535-D)

- [63] Bekshaev, A. & Popov, A. Optical system for Laguerre-Gaussian / Hermite-Gaussian mode conversion. *Proc. SPIE* **4403**, 296–301 (2001). <https://doi.org/10.1117/12.428283>
- [64] Soroko, L. M. *Holography and Coherent Optics*. (Springer, Boston, 1980). <https://doi.org/10.1007/978-1-4684-3420-0>
- [65] Petrov, D. V. Vortex–edge dislocation interaction in a linear medium. *Opt. Commun.*, **188**, 307–312 (2001). [https://doi.org/10.1016/S0030-4018\(01\)00993-2](https://doi.org/10.1016/S0030-4018(01)00993-2)
- [66] Cheng, S. *et al.* Composite spiral zone plate. *IEEE Photon. J.* **11**, 1–11 (2018). <https://doi.org/10.1109/JPHOT.2018.2885004>
- [67] Sabatyan, A. & Behjat, Z. Radial phase modulated spiral zone plate for generation and manipulation of optical perfect vortex. *Opt. Quantum Electron.* **49**, 371 (2017). <https://doi.org/10.1007/s11082-017-1211-4>
- [68] Bekshaev, A. Y. & Karamoch, A. I. Displacements and deformations of a vortex light beam produced by the diffraction grating with embedded phase singularity. *Opt. Commun.* **281**, 3597–3610 (2008). <https://doi.org/10.1016/j.optcom.2008.03.070>
- [69] Anan'ev, Y. A. & Bekshaev, A. Y. Theory of intensity moments for arbitrary light beams. *Opt. Spectrosc.* **76**, 558–568 (1994).
- [70] Bekshaev, A. Y., Mohammed, K. A. & Kurka, I. A. Transverse energy circulation and the edge diffraction of an optical vortex beam. *Appl. Opt.* **53**, B27–B37 (2014). <https://doi.org/10.1364/AO.53.000B27>
- [71] Oemrawsingh, S. S. R. *et al.* Production and characterization of spiral phase plates for optical wavelengths. *Appl. Opt.* **43**, 688–694 (2004). <https://doi.org/10.1364/AO.43.000688>
- [72] Berry, M. V. Optical vortices evolving from helicoidal integer and fractional phase steps. *J. Opt. A Pure Appl. Opt.* **6**, 259 (2004). <https://doi.org/10.1088/1464-4258/6/2/018>
- [73] Kotlyar, V. V. *et al.* Generation of phase singularity through diffracting a plane or Gaussian beam by a spiral phase plate. *J. Opt. Soc. Am. A: Opt. Image Sci. Vis.* **22**(5), 849–861 (2005). <https://doi.org/10.1364/JOSAA.22.000849>
- [74] Bomzon, Z., Biener, G., Kleiner, V. & Hasman, E. Space-variant Pancharatnam–Berry phase optical elements with computer-generated subwavelength gratings. *Opt. Lett.* **27**, 1141–1143 (2002). <https://doi.org/10.1364/OL.27.001141>
- [75] Biener, G., Niv, A., Kleiner, V. & Hasman, E. Formation of helical beams by use of Pancharatnam–Berry phase optical elements. *Opt. Lett.* **27**, 1875–1877 (2002). <https://doi.org/10.1364/OL.27.001875>
- [76] Niv, A., Biener, G., Kleiner, V. & Hasman, E. Manipulation of the Pancharatnam phase in vectorial vortices. *Opt. Express* **14**, 4208–4220 (2006). <https://doi.org/10.1364/OE.14.004208>
- [77] Marucci, L., Manzo, C. & Paparo, D. Optical spin-to-orbital angular momentum conversion in inhomogeneous anisotropic media. *Phys. Rev. Lett.* **96**, 163905 (2006). <https://doi.org/10.1103/PhysRevLett.96.163905>
- [78] Basistiy, I. V., Pas'ko, V. A., Slyusar, V. V., Soskin, M. S. & Vasnetsov, M. V. Synthesis and analysis of optical vortices with fractional topological charges. *J. Opt. A Pure Appl. Opt.* **6**, S166–S169 (2004). <https://doi.org/10.1088/1464-4258/6/5/003>
- [79] Gbur, G. Fractional vortex Hilbert's hotel. *Optica* **3**, 222–225 (2016). <https://doi.org/10.1364/OPTICA.3.000222>
- [80] Freund, I. & Shvartsman, N. Wave-field phase singularities: the sign principle. *Phys. Rev. A* **50**, 5164 (1994). <https://doi.org/10.1103/PhysRevA.50.5164>
- [81] Soskin, M. S., Gorshkov, V. N., Vasnetsov, M. V., Malos, J. T. & Heckenberg, N. R. Topological charge and angular momentum of light beams carrying optical vortices. *Phys. Rev. A* **56**, 4064–4075 (1997). <https://doi.org/10.1103/PhysRevA.56.4064>
- [82] Bialynicki-Birula, I. & Bialynicka-Birula, Z. Rotational frequency shift. *Phys. Rev. Lett.* **78**, 2539–2542 (1997). <https://doi.org/10.1103/PhysRevLett.78.2539>
- [83] Garetz, B. A. Angular Doppler effect. *J. Opt. Soc. Am.* **71**, 609–611 (1981). <https://doi.org/10.1364/JOSA.71.000609>
- [84] Garetz, B. A. & Arnold, S. Variable frequency shifting of circularly polarized laser radiation via a rotating half-wave plate. *Opt. Commun.* **31**, 1–3 (1979). [https://doi.org/10.1016/0030-4018\(79\)90230-X](https://doi.org/10.1016/0030-4018(79)90230-X)
- [85] Simon, R., Kimble, H. J. & Sudarshan, E. C. G. Evolving geometric phase and its dynamical manifestation as a frequency shift: An optical experiment. *Phys. Rev. Lett.* **61**, 19–22 (1988). <https://doi.org/10.1103/PhysRevLett.61.19>
- [86] Bretenaker, F. & Le Floch, A. Energy exchanges between a rotating retardation plate and a laser beam. *Phys. Rev. Lett.* **65**, 2316 (1990). <https://doi.org/10.1103/PhysRevLett.65.2316>
- [87] Courtial, J., Dholakia, K., Robertson, D. A., Allen, L. & Padgett, M. J. Measurement of the rotational frequency shift imparted to a rotating light beam possessing orbital angular momentum. *Phys. Rev. Lett.* **80**, 3217–3219 (1998). <https://doi.org/10.1103/PhysRevLett.80.3217>
- [88] Courtial, J., Robertson, D. A., Dholakia, K., Allen, L. & Padgett, M. J. Rotational frequency shift of a light beam. *Phys. Rev. Lett.* **81**, 4828–4830 (1998). <https://doi.org/10.1103/PhysRevLett.81.4828>
- [89] Bekshaev, A. Ya. *et al.* Observation of rotational Doppler effect with an optical-vortex one-beam interferometer. *Ukr. J. Phys.* **47**, 1035–1040 (2002). <http://archive.ujp.bitp.kiev.ua/files/journals/47/11/471105p.pdf>
- [90] Basistiy, I. V., Bekshaev, A. Y., Vasnetsov, M. V., Slyusar, V. V. & Soskin, M. S. Observation of the rotational Doppler effect for optical beams with helical wave front using spiral zone plate. *JETP Lett.* **76**, 486–489 (2002). <https://doi.org/10.1134/1.1533771>
- [91] Basistiy, I. V., Slyusar, V. V., Soskin, M. S., Vasnetsov, M. V. & Bekshaev, A. Ya. Manifestation of the rotational Doppler effect by use of an off-axis optical vortex beam. *Opt. Lett.* **28**, 1185–1187 (2003). <https://doi.org/10.1364/OL.28.001185>
- [92] Bekshaev, A. & Popov, A. Non-collinear rotational Doppler effect. *Proc. SPIE* **5477**, 55–66 (2004). <https://doi.org/10.1117/12.558759>
- [93] Bekshaev, A. Ya. & Grimblatov, V. M. Energy method of analysis of optical resonators with mirror deformations. *Opt. Spectrosc.* **58**, 707–709 (1985).
- [94] Bekshaev, A. Ya., Grimblatov, V. M. & Kalugin, V. V. *Misaligned Ring Resonator with A Lens-Like Medium*. (Odessa University, 2016). <https://doi.org/10.48550/arXiv.1612.01407>
- [95] Bekshaev, A. Y. Manifestation of mechanical properties of light waves in vortex beam optical systems. *Opt. Spectrosc.* **88**, 904–910 (2000). <https://doi.org/10.1134/1.626898>
- [96] Bekshaev, A. Ya. Mechanical properties of the light wave with phase singularity. *Proc. SPIE* **3904**, 131–139 (1999). <https://doi.org/10.1117/12.370396>
- [97] Bekshaev, A. Ya., Soskin, M. S. & Vasnetsov, M. V. Rotation of arbitrary optical image and the rotational Doppler effect. *Ukr. J. Phys.* **49**, 490–495 (2004). <http://archive.ujp.bitp.kiev.ua/files/journals/49/5/490512p.pdf>
- [98] Vinit'skii, S. I., Derbov, V. L., Dubovik, V. M., Markovski, B. L. & Stepanovskii, Yu. P. Topological phases in quantum mechanics and polarization optics. *Sov. Phys. Usp.* **33**, 403–429 (1990). <https://doi.org/10.1070/PU1990v03n06ABEH002598>
- [99] Bekshaev, A. Ya., Soskin, M. S. & Vasnetsov, M. V. An optical vortex as a rotating body: mechanical features of a singular light beam. *J. Opt. A Pure Appl. Opt.* **6**, S170–S174 (2004). <https://doi.org/10.1088/1464-4258/6/5/004>
- [100] Allen, L. & Padgett, M. J. The Poynting vector in Laguerre-Gaussian beams and the interpretation of their angular momentum density. *Opt. Commun.* **184**, 67–71 (2000). [https://doi.org/10.1016/S0030-4018\(00\)00960-3](https://doi.org/10.1016/S0030-4018(00)00960-3)
- [101] Bekshaev, A. Ya. Transverse rotation of the instantaneous field distribution and the orbital angular momentum of a light beam. *J. Opt. A Pure Appl. Opt.* **11**, 094004 (2009). <https://doi.org/10.1088/1464-4258/11/9/094004>
- [102] Bekshaev, A. Ya. Internal energy flows and instantaneous field of a monochromatic paraxial light beam. *Appl. Opt.* **51**, C13–C16 (2012). <https://doi.org/10.1364/AO.51.000C13>
- [103] Lekner, J. TM, TE, and ‘TEM’ beam modes: exact solutions and their problems. *J. Opt. A Pure Appl. Opt.* **3**, 407–412 (2001). <https://doi.org/10.1088/1464-4258/3/5/314>
- [104] Lekner, J. Phase and transport velocities in particle and electromagnetic beams. *J. Opt. A Pure Appl. Opt.* **4**, 491–499 (2002). <https://doi.org/10.1088/1464-4258/4/5/301>
- [105] Lekner, J. Polarization of tightly focused laser beams. *J. Opt. A Pure Appl. Opt.* **5**, 6–14 (2003). <https://doi.org/10.1088/1464-4258/5/1/302>
- [106] He, H., Friese, M. E. J., Heckenberg, N. R. & Rubinsztein-Dunlop, H. Direct observation of transfer of angular momentum to absorptive particles from a laser beam with a phase singularity. *Phys. Rev. Lett.* **75**, 826–829 (1995). <https://doi.org/10.1103/PhysRevLett.75.826>
- [107] Rubinsztein-Dunlop, H., Nieminen, T. A., Friese, M. E. J. & Heckenberg, N. R. Optical trapping of absorbing particles. *Adv.*

- Quantum Chem.* **30**, 469–492 (1998).
[https://doi.org/10.1016/S0065-3276\(08\)60523-7](https://doi.org/10.1016/S0065-3276(08)60523-7)
- [108] Gahagan, K. T. & Swartzlander, G. A. Optical vortex trapping of particles. *Opt. Lett.* **21**, 827–829 (1996).
<https://doi.org/10.1364/OL.21.000827>
- [109] Gahagan, K. T. & Swartzlander, G. A. Trapping of low-index microparticles in an optical vortex. *J. Opt. Soc. Am. B* **15**, 524–534 (1998). <https://doi.org/10.1364/JOSAB.15.000524>
- [110] Simpson, N. B., McGloin, D., Dholakia, K., Allen, L. & Padgett, M. J. Optical tweezers with increased axial trapping efficiency. *J. Mod. Opt.* **45**, 1943–1949 (1998).
<https://doi.org/10.1080/09500349808231712>
- [111] Simpson, N. B., Allen, L. & Padgett, M. J. Optical tweezers and optical spanners with Laguerre Gaussian modes. *J. Mod. Opt.* **43**, 2485–2491 (1996). <https://doi.org/10.1080/09500349608230675>
- [112] O’Neil, A. T. & Padgett, M. J. Three-dimensional optical confinement of micron-sized metal particles and the decoupling of the spin and orbital angular momentum within an optical spanner. *Opt. Commun.* **185**, 139–143 (2000).
[https://doi.org/10.1016/S0030-4018\(00\)00989-5](https://doi.org/10.1016/S0030-4018(00)00989-5)
- [113] Higurashi, E., Sawada, R. & Ito, T. Optically induced angular alignment of trapped birefringent micro-objects by linearly polarized light. *Phys. Rev. E* **59**, 3676–3681 (1999).
<https://doi.org/10.1103/PhysRevE.59.3676>
- [114] Friese, M. E. J., Rubinsztein-Dunlop, H., Gold, J., Hagberg, P. & Hanstorp, D. Optically driven micromachine elements. *Appl. Phys. Lett.* **78**, 547–549 (2001). <https://doi.org/10.1063/1.1339995>
- [115] Paterson, L. et al. Controlled rotation of optically trapped microscopic particles. *Science* **292**, 912–914 (2001).
<https://doi.org/10.1126/science.1058591>
- [116] Grier, D. G. A revolution in optical manipulation. *Nature* **424**, 810–816 (2003). <https://doi.org/10.1038/nature01935>
- [117] Bowman, R. W. & Padgett, M. J. Optical trapping and binding. *Rep. Prog. Phys.* **76**, 026401 (2013).
<https://doi.org/10.1088/0034-4885/76/2/026401>
- [118] Padgett, M. & Bowman, R. Tweezers with a twist. *Nat. photonics* **5**, 343–348 (2011). <https://doi.org/10.1038/nphoton.2011.81>
- [119] Jack, Ng., Lin, Zh. & Chan, C. T. Theory of optical trapping by an optical vortex beam. *Phys. Rev. Lett.* **104**, 103601 (2010).
<https://doi.org/10.1103/PhysRevLett.104.103601>
- [120] Yuehan, T. et al. Multi-trap optical tweezers based on composite vortex beams. *Opt. Commun.* **485**, 126712 (2021).
<https://doi.org/10.1016/j.optcom.2020.126712>
- [121] Chun-Fu, K. & Chu, S.-Ch. Numerical study of the properties of optical vortex array laser tweezers. *Opt. Express* **21**, 26418–26431 (2013). <https://doi.org/10.1364/OE.21.026418>
- [122] Mokhun, I. I. Introduction to Linear Singular Optics. in *Optical Correlation Techniques and Applications* (ed. Angelsky, O.) 1–132 (Bellingham, SPIE Press PM168, 2007).
<https://doi.org/10.1117/3.714999.ch1>
- [123] Mokhun, I. I. Introduction to Linear Singular Optics (Chernivtsi National University, 2012) (In Russian)
- [124] Angelsky, O. V., Besaga, R. N. & Mokhun, I. I. Appearance of wave front dislocations under interference among beams with simple wave fronts. *Proc. SPIE* **3317**, 97–100 (1997).
<https://doi.org/10.1117/12.295666>
- [125] O’Holleran, K., Padgett, M. J. & Dennis, M. R. Topology of optical vortex lines formed by the interference of three, four, and five plane waves. *Opt. Express* **14**, 3039–3044 (2006).
<https://doi.org/10.1364/OE.14.003039>
- [126] Xavier, J., Vyas, S., Senthilkumaran, P. & Joseph, J. Tailored complex 3D vortex lattice structures by perturbed multiples of three-plane waves. *Appl. Opt.* **51**, 1872–1878 (2012).
<https://doi.org/10.1364/AO.51.001872>
- [127] Kapoor, A., Kumar, M., Senthilkumaran, P. & Joseph, J. Optical vortex array in spatially varying lattice. *Opt. Commun.* **365**, 99–102 (2016). <https://doi.org/10.1016/j.optcom.2015.11.074>
- [128] Xavier, J., Vyas, S., Senthilkumaran, P. & Joseph, J. Complex 3D vortex lattice formation by phase-engineered multiple beam interference. *Int. J. Opt.* **2012**, 863875 (2012).
<https://doi.org/10.1155/2012/863875>
- [129] Galvez, E. J., Rojec, B. L., Beach, K. & Cheng, X. C-point singularities in Poincaré Beams (2014). <http://citeseerx.ist.psu.edu/viewdoc/download?doi=10.1.1.712.1192&rep=rep1&type=pdf>
- [130] Mokhun, A. I., Soskin, M. S. & Freund, I. Elliptic critical points in paraxial optical fields. *Opt. Commun.* **208**, 223–253 (2002).
[https://doi.org/10.1016/S0030-4018\(02\)01585-7](https://doi.org/10.1016/S0030-4018(02)01585-7)
- [131] Mokhun, I., Galushko, Yu., Kharitonova, Ye., Viktorovskaya, Yu. & Khrobatin, R. Elementary heterogeneously polarized field modeling. *Opt. Lett.* **36**, 2137–2139 (2011).
<https://doi.org/10.1364/OL.36.002137>
- [132] Angelsky, O. V., Dominikov, N. N., Maksimyak, P. P. & Tudor, T. Experimental revealing of polarization waves. *Appl. Opt.* **38**, 3112–3117 (1999). <https://doi.org/10.1364/AO.38.003112>
- [133] Angelsky, O. V., Hanson, S. G., Zenkova, C. Yu., Gorsky, M. P. & Gorodin’ska, N. V. On polarization metrology (estimation) of the degree of coherence of optical waves. *Opt. Express* **17**, 15623–15634 (2009). <https://doi.org/10.1364/OE.17.015623>
- [134] Mokhun, I., Khrobatin, R. & Viktorovskaya, Ju. The behavior of the Poynting vector in the area of elementary polarization singularities. *Opt. Appl.* **37**, 261–277 (2007).
- [135] Khrobatin, R. & Mokhun, I. Shift of application point of angular momentum in the area of elementary polarization singularity. *J. Opt. A Pure Appl. Opt.* **10**, 064015 (2008).
<https://doi.org/10.1088/1464-4258/10/6/064015>
- [136] Angelsky, O. V., Besaga, R. N., Mokhun, I. I., Soskin, M. S. & Vasnetsov, M. V. Singularities in vectorial fields. *Proc. SPIE* **3904**, 40–55 (1999). <https://doi.org/10.1117/12.370443>
- [137] Mokhun, I. I., Arkhlyuk, A., Galushko, Yu., Kharitonova, Ye., & Viktorovskaya, Ju. Experimental analysis of the Poynting vector characteristics. *Appl. Opt.* **51**, C158–C162 (2012).
<https://doi.org/10.1364/AO.51.00C158>
- [138] Mokhun, I., Arkhlyuk, A. D., Galushko, Yu., Kharitonova, Ye. & Viktorovskaya, Yu. Angular momentum of an incoherent Gaussian beam. *Appl. Opt.* **53**, B38–B42 (2014).
<https://doi.org/10.1364/AO.53.000B38>
- [139] Andronov, A. A., Vitt, A. A. & Khaikin, S. E. *Theory of Oscillators* (Pergamon Press, 1966).
- [140] Bekshaev, A. Ya. Spin angular momentum of inhomogeneous and transversely limited light beams. *Proc. SPIE* **6254**, 56–63 (2006).
<https://doi.org/10.1117/12.679902>
- [141] O’Neil, A. T., MacVicar, I., Allen, L. & Padgett, M. J. Intrinsic and extrinsic nature of the orbital angular momentum of a light beam. *Phys. Rev. Lett.* **88**, 053601 (2002).
<https://doi.org/10.1103/PhysRevLett.88.053601>
- [142] Bekshaev, A. Ya., Soskin, M. S. & Vasnetsov, M. V. Optical vortex symmetry breakdown and decomposition of the orbital angular momentum of light beams. *J. Opt. Soc. Amer. A* **20**, 1635–1643 (2003). <https://doi.org/10.1364/JOSAA.20.001635>
- [143] Belinfante, F. J. On the current and the density of the electric charge, the energy, the linear momentum and the angular momentum of arbitrary fields. *Physica* **7**, 449 (1940).
[https://doi.org/10.1016/S0031-8914\(40\)90091-X](https://doi.org/10.1016/S0031-8914(40)90091-X)
- [144] Bliokh, K. Y., Dressel, J. & Nori, F. Conservation of the spin and orbital angular momenta in electromagnetism. *New J. Phys.* **16**, 093037 (2014). <https://doi.org/10.1088/1367-2630/16/9/093037>
- [145] Angelsky, O. V. et al. Investigation of optical currents in coherent and partially coherent vector fields. *Opt. Express* **19**, 660–672 (2011). <https://doi.org/10.1364/OE.19.000660>
- [146] Zenkova, C. Yu., Gorsky, M. P., Maksimyak, P. P. & Maksimyak, A. P. Optical currents in vector fields. *App. Opt.* **50**, 1105–1112 (2011) <https://doi.org/10.1364/AO.50.001105>
- [147] Angelsky, O. V., Zenkova, C. Yu., Hanson, S. G. & Zheng, J. Extraordinary manifestation of evanescent wave in biomedical application. *Front. Phys.* **8**, 159 (2020).
<https://doi.org/10.3389/fphy.2020.00159>
- [148] Angelsky, O., Bekshaev, A., Dragan, G., Maksimyak, P., Zenkova, C.Y. & Zheng, J., Structured light control and diagnostics using optical crystals. *Front. Phys.* **9**, 368 (2021).
<https://doi.org/10.3389/fphy.2021.715045>
- [149] Angelsky, O. *Introduction to Singular Correlation Optics*. (SPIE Press, 2019).
- [150] Allen, L. & Padgett, M. J. Response to question #79. Does a plane wave carry spin angular momentum? *Am. J. Phys.* **70**, 567–568 (2002). <https://doi.org/10.1119/1.1456075>
- [151] Pfeifer, R. N. C., Nieminen, T. A., Heckenberg, N. R. & Rubinsztein-Dunlop, H. Optical tweezers and paradoxes in electromagnetism. *J. Opt.* **13**, 044017 (2011).
<https://doi.org/10.1088/2040-8978/13/4/044017>

- [152] Stewart, A. M. Angular momentum of the electromagnetic field: the plane wave paradox resolved. *Eur. J. Phys.* **26**, 635–641 (2005). <https://doi.org/10.1088/0143-0807/26/4/008>
- [153] Bekshaev, A. Ya. “Spin” and “Orbital” Flows in A Circularly Polarized Paraxial Beam: Orbital Rotation Without Orbital Angular Momentum. <https://arxiv.org/ftp/arxiv/papers/0908/0908.2526.pdf> (2009).
- [154] Bekshaev, A. & Vasnetsov, M. Vortex Flow of Light: “Spin” and “Orbital” Flows in a Circularly Polarized Paraxial Beam. in *Twisted Photons. Applications of Light with Orbital Angular Momentum* (eds. Torres, J. P. & Torner, L.) chapter 2 (Weinheim: Wiley-VCH, 2011). <https://doi.org/10.1002/9783527635368.ch2>
- [155] Bekshaev, A. & Soskin, M. Transverse energy flows in vectorial fields of paraxial light beams. *Proc. SPIE* **6729**, 67290G (2007). <https://doi.org/10.1117/12.751952>
- [156] Dienerowitz, M., Mazilu, M. & Dholakia, K. Optical manipulation of nanoparticles: a review. *J. Nanophotonics* **2**, 021875 (2008). <https://doi.org/10.1117/1.2992045>
- [157] Gouesbet, G. T-matrix methods for electromagnetic structured beams: a commented reference database for the period 2014–2018. *J. Quant. Spectrosc. Radiat. Transf.* **230**, 247–281 (2019). <https://doi.org/10.1016/j.jqsrt.2019.04.004>
- [158] Nieminen, T. A., Loke, V. L., Stilgoe, A. B., Heckenberg, N. R., & Rubinsztein-Dunlop, H. T-matrix method for modelling optical tweezers. *J. Mod. Opt.* **58**, 528–544 (2011). <https://doi.org/10.1080/09500340.2010.528565>
- [159] Bekshaev, A. Y., Bliokh, K. Y. & Nori, F. Mie scattering and optical forces from evanescent fields: A complex-angle approach. *Opt. Express* **21**, 7082–7095 (2013). <https://doi.org/10.1364/OE.21.007082>
- [160] Angelsky, O., Bekshaev, A., Maksimyak, P., Maksimyak, A. & Hanson, S. Measurement of small light absorption in microparticles by means of optically induced rotation. *Opt. Express* **23**, 7152–7163 (2015). <https://doi.org/10.1364/OE.23.007152>
- [161] Bekshaev A. Ya., Angelsky O. V., Sviridova S. V. & Zenkova C. Yu. Mechanical action of inhomogeneously polarized optical fields and detection of the internal energy flows. *Adv. Opt. Technol.* **2011**, 723901 (2011). <https://doi.org/10.1155/2011/723901>
- [162] Bekshaev, A. Ya., Angelsky, O. V., Hanson, S. G. & Zenkova, C. Yu. Scattering of inhomogeneous circularly polarized optical field and mechanical manifestation of the internal energy flows. *Phys. Rev. A* **86**, 023847-10 (2012). <https://doi.org/10.1103/PhysRevA.86.023847>
- [163] Bohren, C. F. & Huffman, D. R. *Absorption and Scattering of Light by Small Particles*. (Wiley-VCH, 1983).
- [164] Bekshaev, A. Y. Subwavelength particles in an inhomogeneous light field: Optical forces associated with the spin and orbital energy flows. *J. Opt.* **15**, 044004 (2013). <https://doi.org/10.1088/2040-8978/15/4/044004>
- [165] Bliokh, K. Y., Bekshaev, A. Y. & Nori, F. Extraordinary momentum and spin in evanescent waves. *Nat. Commun.* **5**, 3300 (2014). <https://doi.org/10.1038/ncomms4300>
- [166] Liberal, I., Ederra, I., Gonzalo, R. & Ziolkowski, R. W. Electromagnetic force density in electrically and magnetically polarizable media. *Phys. Rev. A* **88**, 053808 (2013). <https://doi.org/10.1103/PhysRevA.88.053808>
- [167] Nieto-Vesperinas, M., Saenz, J. J., Gomez-Medina, R. & Chantada, L. Optical forces on small magnetodielectric particles. *Opt. Express* **18**, 11428–11443 (2010). <https://doi.org/10.1364/OE.18.011428>
- [168] Canaguier-Durand, A., Cuche, A., Cyriaque, G. & Ebbesen, T. W. Force and torque on an electric dipole by spinning light fields. *Phys. Rev. A* **88**, 033831 (2013). <https://doi.org/10.1103/PhysRevA.88.033831>
- [169] Bliokh, K. Y., Bekshaev, A. Y. & Nori, F. Dual electromagnetism: helicity, spin, momentum and angular momentum. *New J. Phys.* **15**, 033026 (2013). <https://doi.org/10.1088/1367-2630/15/3/033026>
- [170] Xu, X. & Nieto-Vesperinas, M. Azimuthal imaginary Poynting momentum density. *Phys. Rev. Lett.* **123**, 233902 (2019). <https://doi.org/10.1103/PhysRevLett.123.233902>
- [171] Nieto-Vesperinas, M. & Xu, X. Reactive helicity and reactive power in nanoscale optics: Evanescent waves. Kerker conditions. Optical theorems and reactive dichroism. *Phys. Rev. Res.* **3**, 043080 (2021). <https://doi.org/10.1103/PhysRevResearch.3.043080>
- [172] Bekshaev, A., Kontush, S., Popov, A. & Van Grieken, R. Application of light beams with non-zero angular momentum in optical study of micrometer-size aerosol particles. *Proc. SPIE* **4403**, 287–295 (2001). <https://doi.org/10.1117/12.428282>
- [173] Bekshaev, A. Abraham-Based Momentum and Spin of Optical Fields Under Conditions of Total Reflection. <https://arxiv.org/ftp/arxiv/papers/1710/1710.01561.pdf> (2017).
- [174] Angelsky, O. V. et al. Orbital rotation without orbital angular momentum: mechanical action of the spin part of the internal energy flow in light beams. *Opt. Express* **20**, 3563–3571 (2012). <https://doi.org/10.1364/OE.20.003563>
- [175] Angelsky, O.V. et al. Circular motion of particles suspended in a Gaussian beam with circular polarization validates the spin part of the internal energy flow. *Opt. Express* **20**, 11351–11356 (2012). <https://doi.org/10.1364/OE.20.011351>
- [176] Angelsky, O. V., Bekshaev, A. Ya., Maksimyak, P. P. & Polyanskiy, P. V. Internal energy flows and optical trapping. *Opt. Photonic News* **25**, 20–21 (2014).
- [177] Bekshaev, A. Y., Bliokh, K. Y. & Nori, F. Transverse spin and momentum in two-wave interference. *Phys. Rev. X* **5**, 011039 (2015). <https://doi.org/10.1103/PhysRevX.5.011039>
- [178] Antognozzi, M. et al. Direct measurements of the extraordinary optical momentum and transverse spin-dependent force using a nano-cantilever. *Nat. Phys.* **12**, 731–735 (2016). <https://doi.org/10.1038/nphys3732>
- [179] Bekshaev, A. Y. Dynamical characteristics of an electromagnetic field under conditions of total reflection. *J. Opt.* **2**, 045604 (2018). <https://doi.org/10.1088/2040-8986/aab035>
- [180] Bliokh, K. Y. & Nori, F. Transverse spin of a surface polariton. *Phys. Rev. A* **85**, 061801 (2012). <https://doi.org/10.1103/PhysRevA.85.061801>
- [181] Bliokh, K. Y., Smimova, D. & Nori, F. Quantum spin Hall effect of light. *Science* **348**, 1448–1451 (2015). <https://doi.org/10.1126/science.aaa9519>
- [182] Bliokh, K. Y. Rodríguez-Fortuño, F. J., Nori, F. & Zayats, A. V. Spin-orbit interactions of light. *Nat. Photonics* **9**, 796 (2015). <https://doi.org/10.1038/nphoton.2015.201>
- [183] Skelton, S. E. et al. Evanescent wave optical trapping and sktransport of micro and nanoparticles on tapered optical fibers. *J. Quant. Spectrosc. Radiat. Transf.* **113**, 2512–2520 (2012). <https://doi.org/10.1016/j.jqsrt.2012.06.005>
- [184] Chang, S., Kim, J. T., Jo, J. H. & Lee, S. S. Optical force on a sphere caused by the evanescent field of a Gaussian beam; effects of multiple scattering. *Opt. Commun.* **139**, 252–261 (1997). [https://doi.org/10.1016/S0030-4018\(97\)00144-2](https://doi.org/10.1016/S0030-4018(97)00144-2)
- [185] Song, Y. G., Han, B. M. & Chang, S. Force of surface plasmon-coupled evanescent fields on Mie particles. *Opt. Commun.* **198**, 7–19 (2001). [https://doi.org/10.1016/S0030-4018\(01\)01484-5](https://doi.org/10.1016/S0030-4018(01)01484-5)
- [186] Angelsky, O. V. et al. Influence of evanescent wave on birefringent microplates. *Opt. Express* **25**, 2299–2311 (2017). <https://doi.org/10.1364/OE.25.002299>
- [187] Zenkova C. Yu., Ivanskyi, D. I. & Kiyashchuk, T. V. Optical torques and forces in birefringent microplate. *Opt. Appl.* **47**, 1–11 (2017). <https://doi.org/10.5277/oa170313>
- [188] Angelsky, O. V., Zenkova, C. Yu. & Ivansky, D. I. Mechanical action of the transverse spin momentum of an evanescent wave on gold nanoparticles in biological objects media. *J. Optoelectron. Adv. Mater.* **20**, 217–226 (2018).
- [189] Angelsky, O.V. et al. Controlling and manipulation of red blood cells by evanescent waves. *Opt. Appl.* **49**, 597–611 (2019). <https://doi.org/10.37190/oa190406>
- [190] Angelsky, O. V. et al. Peculiarities of control of erythrocytes moving in an evanescent field. *J. Biomed. Opt.* **24**, 055002 (2019). <https://doi.org/10.1117/1.JBO.24.5.055002>
- [191] Angelsky, O.V. et al. Peculiarities of energy circulation in evanescent field. Application for red blood cells. *Opt. Mem. Neural Netw. (Inf. Opt.)* **28**, 11–20 (2019). <https://doi.org/10.3103/S1060992X19010028>
- [192] Berry, M. V. & Dennis, M. R. The optical singularities of birefringent dichroic chiral crystals. *Proc. R. Soc. Lond.* **459**, 1261 (2003). <https://doi.org/10.1098/rspa.2003.1155>
- [193] Bliokh, K. Y. & Nori, F. Characterizing optical chirality. *Phys. Rev. A* **83**, 021803(R) (2011). <https://doi.org/10.1103/PhysRevA.83.021803>
- [194] Desyatnikov, A. S., Sukhorukov, A. A. & Kivshar, Y. S. Azimuthons: spatially modulated vortex solitons. *Phys. Rev. Lett.* **95**, 20, 203904 (2005). <https://doi.org/10.1103/PhysRevLett.95.203904>

- [195] Kivshar, Y. S. Vortex solitons and rotating azimuthons in nonlinear media. *Topologica* **2**, 005 (2009). <https://doi.org/10.3731/topologica.2.005>
- [196] Bekshaev, A., Angelsky, O. & Hanson, S.G. Transformations and Evolution of Phase Singularities in Diffracted Optical Vortices. in *Advances in Optics: Reviews, Book Series Vol. 1* (ed. Yurish, S. Y.) 345–385 (International Frequency Sensor Association (IFSA), Spain, 2018). http://www.sensorsportal.com/HTML/BOOKSTORE/Advances_in_Optics_Vol_1.pdf
- [197] Bekshaev, A., Chernykh, A., Khoroshun, A. & Mikhaylovskaya, L. Singular skeleton evolution and topological reactions in edge-diffracted circular optical-vortex beams. *Opt. Commun.* **397**, 72–83 (2017). <https://doi.org/10.1016/j.optcom.2017.03.062>
- [198] Bekshaev, A., Chernykh, A., Khoroshun, A. & Mikhaylovskaya, L. Localization and migration of phase singularities in the edge-diffracted optical-vortex beams. *J. Opt.* **18** 024011 (2016). <https://doi.org/10.1088/2040-8978/18/2/024011>
- [199] Bekshaev, A., Khoroshun, A. & Mikhaylovskaya, L. Transformation of the singular skeleton in optical-vortex beams diffracted by a rectilinear phase step. *J. Opt.* **21**, 084003 (2019). <https://doi.org/10.1088/2040-8986/ab2c5b>
- [200] Bekshaev, A. Spin-orbit interaction of light and diffraction of polarized beams. *J. Opt.* **19**, 085602 (2017). <https://doi.org/10.1088/2040-8986/aa746a>
- [201] Fedoseyev, V. G. Spin-independent transverse shift of the centre of gravity of a reflected and of a refracted light beam. *Opt. Commun.* **193**, 9–18 (2001). [https://doi.org/10.1016/S0030-4018\(01\)01262-7](https://doi.org/10.1016/S0030-4018(01)01262-7)
- [202] Okuda, H. & Sasada, H. Significant deformations and propagation variations of Laguerre-Gaussian beams reflected and transmitted at a dielectric interface. *J. Opt. Am. A: Opt. Image Sci. Vis.* **25**, 881–890 (2008). <https://doi.org/10.1364/JOSAA.25.000881>
- [203] Bekshaev, A. Ya. & Popov, A. Yu. Method of light beam orbital angular momentum evaluation by means of space-angle intensity moments. *Ukr. J. Phys. Opt.* **3**, 249–257 (2002). <https://doi.org/10.3116/16091833/3/4/249/2002>
- [204] Bekshaev, A. Ya. Oblique section of a paraxial light beam: criteria for azimuthal energy flow and orbital angular momentum. *J. Opt. A Pure Appl. Opt.* **11**, 094003 (2009). <https://doi.org/10.1088/1464-4258/11/9/094003>
- [205] Bekshaev, A. Ya. Improved theory for the polarization-dependent transverse shift of a paraxial light beam in free space. *Ukr. J. Phys. Opt.* **12**, 10–18 (2011). <https://doi.org/10.3116/16091833/12/1/10/2011>
- [206] Bekshaev, A. Ya. Polarization-dependent transformation of a paraxial beam upon reflection and refraction: A real-space approach. *Phys. Rev. A* **85**, 023842 (2012). <https://doi.org/10.1103/PhysRevA.85.023842>
- [207] Bliokh, K. Y. & Aiello, A. Goos-Hänchen and Imbert-Fedorov beam shifts: an overview. *J. Opt.* **15**, 014001 (2013). <https://doi.org/10.1088/2040-8978/15/1/014001>